UNIVERSITY OF OKLAHOMA

GRADUATE COLLEGE

STUDY ON THE MECHANICAL AND THERMAL PROPERTIES OF CLASS G CEMENT COMPOSITES

A THESIS

SUBMITTED TO THE GRADUATE FACULTY

in partial fulfillment of the requirements for the

Degree of

MASTER OF SCIENCE

By

MIGUEL LEONARDO ROMERO TELLEZ

Norman, Oklahoma

2023

STUDY ON THE MECHANICAL AND THERMAL PROPERTIES OF CLASS G CEMENT COMPOSITES

A THESIS APPROVED FOR THE

MEWBOURNE SCHOOL OF PETROLEUM AND GEOLOGICAL ENGINEERING

BY THE COMMITTEE CONSISTING OF

Dr. Catalin Teodoriu, Chair

Dr. Ahmed Ramadan

Dr. Hamidreza Karami

ACKNOWLEDGEMENTS

I extend my heartfelt gratitude to Dr. Catalin Teodoriu for believing in my potential and offering me the invaluable chance to serve as his research assistant during my master's program at the University of Oklahoma. His trust in me empowered me to showcase my capabilities and contribute to meaningful research. Additionally, I am deeply appreciative of Dr. Teodoriu for serving as a mentor and providing me with guidance throughout this journey, ultimately enabling me to achieve a significant milestone in my academic and professional aspirations. Moreover, he has become a really special friend during this process.

I would like to express my sincere gratitude to my parents Miguel and Amalia, and my brother Flim who have always supported me in many ways during this tough process, making this journey a better and more remarkable one, likewise, to my cousin Javier who gave me this unique opportunity.

Thanks to my friends and colleagues, who have been cheering and helping me up during these last two years. Thanks to Camila, who helped me to start this journey, without her this would not have been possible.

Finally, thanks to the University of Oklahoma and Mewbourne School of Geological and Petroleum Engineering and the amazing staff.

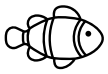

Miguel Romero Tellez

Content

Figures

Tables

Equations

Abstract

Nowadays the consumption of hydrocarbons such as oil and gas are higher than ever before, for that reason, the world is constantly looking for the development of new oil formations that were not accessible before due to the lack of technology for high-pressure and high-temperature reservoirs, being the trigger of new well construction materials that can achieve the new requirements that the industry currently needs. Simultaneously, as the oil and gas industry endeavors to satisfy this growing demand for hydrocarbons, there's a concerted effort to transition towards a more sustainable, environmentally friendly future.

For this reason, the oil and gas industry is moving to carbon-neutral alternatives to materials like cement, that is fundamental in the operation since provides well integrity, which currently has a significant carbon footprint. Cement production accounts for a substantial portion of CO_2 emissions, the production of one kilogram of cement send one kilogram of CO_2 to the atmosphere, contributing to approximately 9% of annual CO_2 emissions produced by humans, underlining the urgency to find greener alternatives.

One of the materials that aligns with the new goals the oil and gas industry is trying to achieve regarding CO_2 emissions and have the desirable characteristic to develop slurries for well cementing are geopolymers. It is a relatively cheap material that is characterized by having a high resistance to acidic environments, high compressive strength, and a low carbon footprint due to the fact is a waste material from other industrial processes.

This thesis focuses on the experimental testing and analysis of the compressive strength of neat class G cement, as well as class G cement with the addition of class F fly ash at different percentages (10%, 20% and 30% were the cement composites selected, above 30% the cement

slurries were not able to be mixed, hence the study stopped at 30% fly ash by weight of cement) at both room and high temperature. Additionally, the characterization and analysis of the same class G cement composites but with the addition of sodium hydroxide to the mixture cured at high temperature. Similarly, the research aimed to experimentally test and analyze the thermal properties of neat class G cement and class G cement composites with the addition of fly ash at different percentages, cured at room temperature, to assess their thermal properties. All of the tests done in this research were conducted for a period of 28 days.

In conclusion, this research reveals that increasing the percentage of fly ash in class G cement composites directly enhances compressive strength consistently across varying environmental conditions. On the other hand, the addition of sodium hydroxide negatively impacts compressive strength by altering pH levels and hindering the formation of critical components, highlighting its adverse effect on cement properties. Finally, the results of the thermal properties were not conclusive when the Keithley 2400 meter with TPS-3 was used suggesting the need of a longer period of time for testing to ensure the stabilization of the values to finally lead to a conclusion. Whereas the results obtained using the Thermtest Portable Measurement Platform −2 concluded that the more fly ash incorporated into the class G cement sample the more is going to be the increment of the thermal conductivity, this being true up to 20% fly ash added by weight of cement. When 30% fly ash by weight of cement was added it was possible to see a slight decrease of this property.

1 Introduction.

This chapter addresses the main ideas that have been examined in the research thesis, providing a complete outline and explanation of the topic at hand. Subsequently, the key objectives aimed at addressing this topic are introduced. Ultimately, the scope of research to achieve the proposed objectives is clarified.

1.1 Problem statement.

Over the last 30 years, the population of the world has increased dramatically, surpassing three times the population in the mid-1900s. from an estimate of 2.5 billion in 1950 to 8 billion by mid-November 2022, increasing 2 billion since 1998 and 1 billion since 2010. Projections have suggested that the global population will add another 2 billion during the following three decades, reaching 9.7 billion by 2050, with a peak of 10.4 billion people around the mid-2080s (United Nations, 2023) as seen in **Figure 1.**

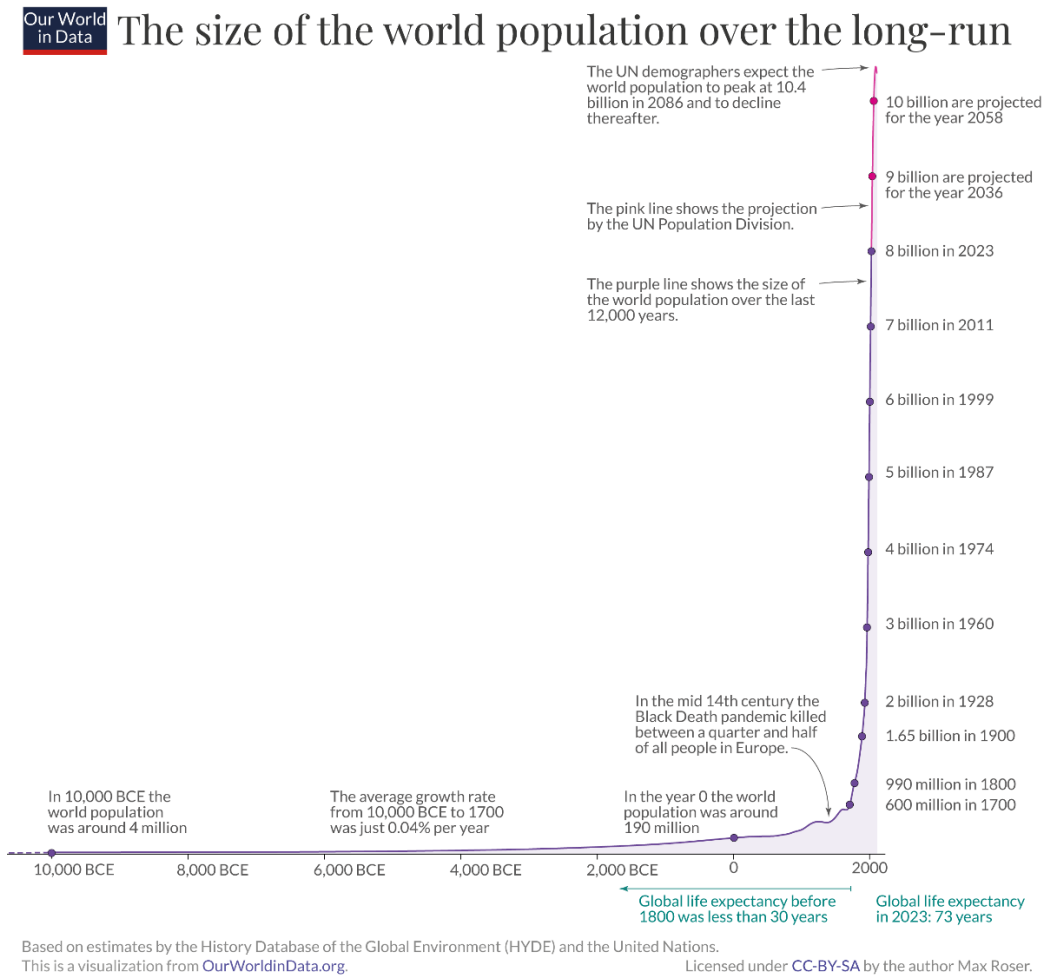

Figure 1. World population growth (United Nations, 2023).

According to the U.S. Energy Information Administration (EIA), the growth in worldwide power consumption is outpacing the increase in the population around the globe as seen in **Figure 2.** which is resulting in an increase in the average amount of electricity consumed per person (also known as per capita electricity consumption) (Energy information administration, 2023).

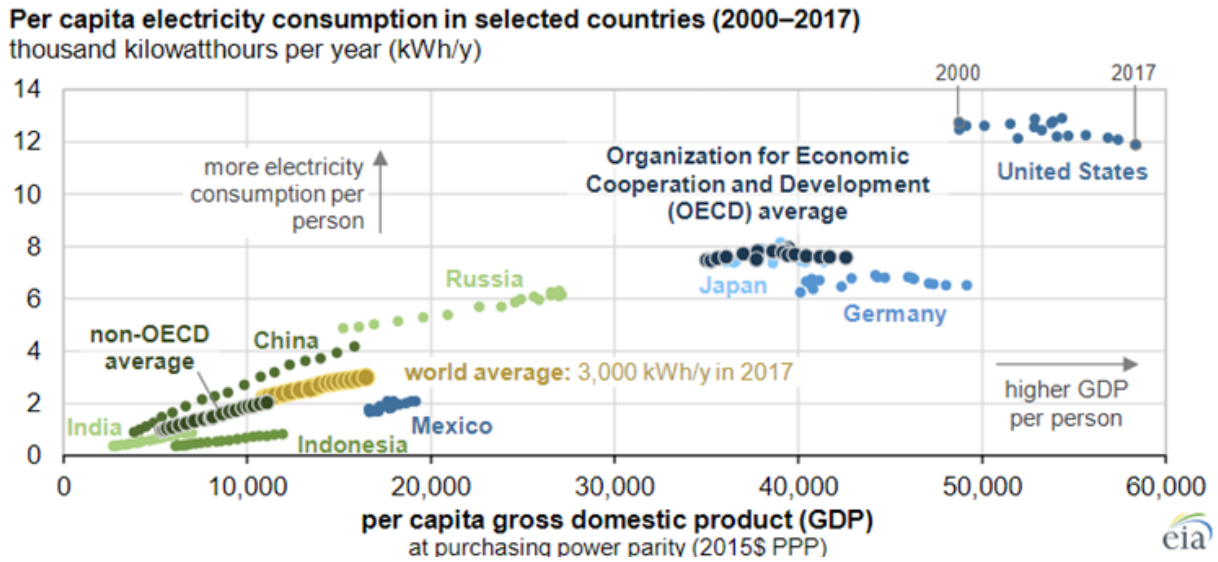

Figure 2. Per capita electricity consumption in selected countries (EIA, 2023).

However, global energy consumption is currently experiencing a major shift in the primary energy sources. Historically, oil and gas have played an important role, accounting for more than 45% of worldwide energy consumption and being the dominant sources in 2020(BP, 2022.). Nevertheless, this dominancy is steadily declining, and it is expected to make up less than 25% of worldwide energy use by 2050. The forecast made by BP (BP, 2022.) shows that by 2030 renewable energy will surpass energy that is produced by burning coal, likewise, this shift is going to be followed by the rising of renewable energy against oil and gas by 2035, having the largest share of participation as depicted on **Figure 3.**

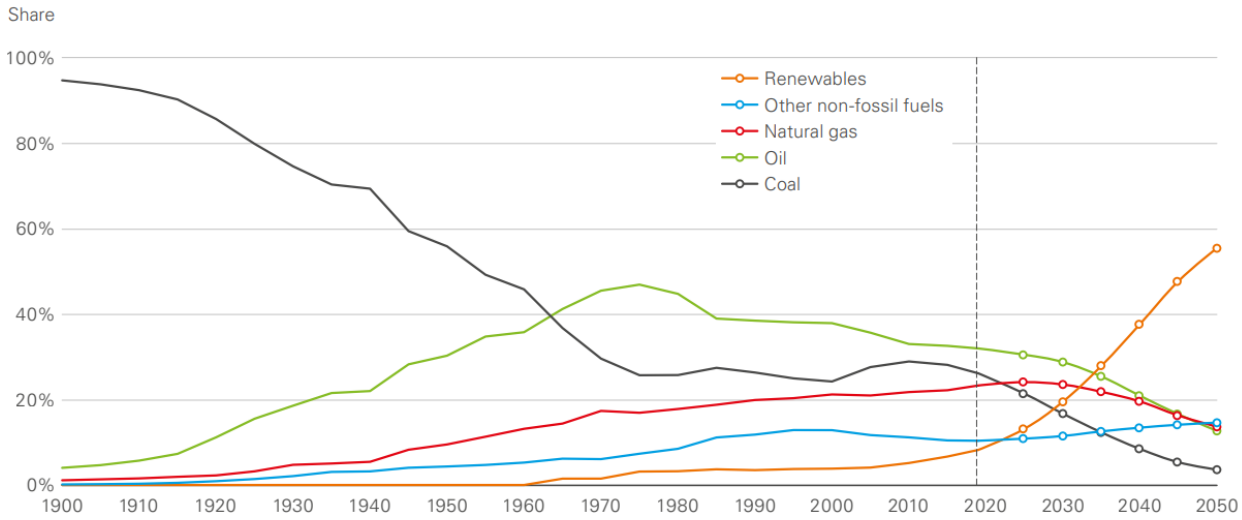

Figure 3. share of primary energy (BP, 2022).

Nonetheless, while oil and gas are going to eventually decrease their share participation in the energy market, different than decrease the production of this commodity, the energy produced through these is going to still have an important role in supplying the demand for energy. Nowadays, in the United States of America, there are over 900.000 wells that are currently producing oil (EIA, 2022) as **Figure 4**, that is why the development of new technologies is fundamental to ensure the longevity of those wells and the new ones, maintaining their integrity while producing oil and gas, and for its possible repurposing to geothermal energy or carbon capture sequestration, until an eventual abandonment of the well.

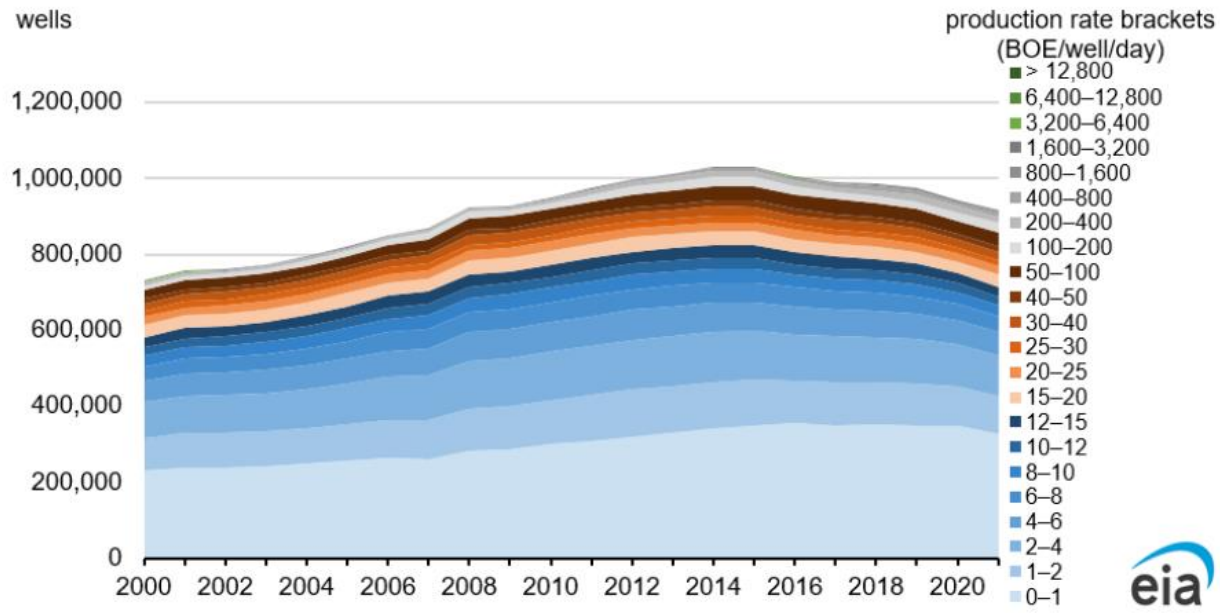

Figure 4. Wells by production rate in the U.S. (EIA, 2022).

Something that needs to be understood is the drilling and completion operations of a well, those operations involve an intensive capital investment and a complex execution which are done in order to connect the targeted formation with the surface, allowing to use that formation depending on the operation that is aimed for, that can go from extraction of oil and gas, injection of carbon dioxide for enhanced oil recovery or carbon capture sequestration, injection of water for water flooding or for geothermal purposes, among others.

As a consequence of the above drilling and completion of new wells will continue to play an important role in the realm of the extraction of those resources, which is driving the evolution of technology holding significance in effectively addressing the challenges associated with accessing the diversity of resources mentioned earlier. These challenges encompass complex formations characterized by elevated pressures and elevated temperatures, the drilling of extremely long lateral wells as seen in **Figure 5** where in the year 2000 the total of lateral wells producing

oil and gas was less than 10,000 in contrast to the over 160,000 wells by 2021 (EIA, 2022), and hostile environments that directly affect the durability of cement and casing.

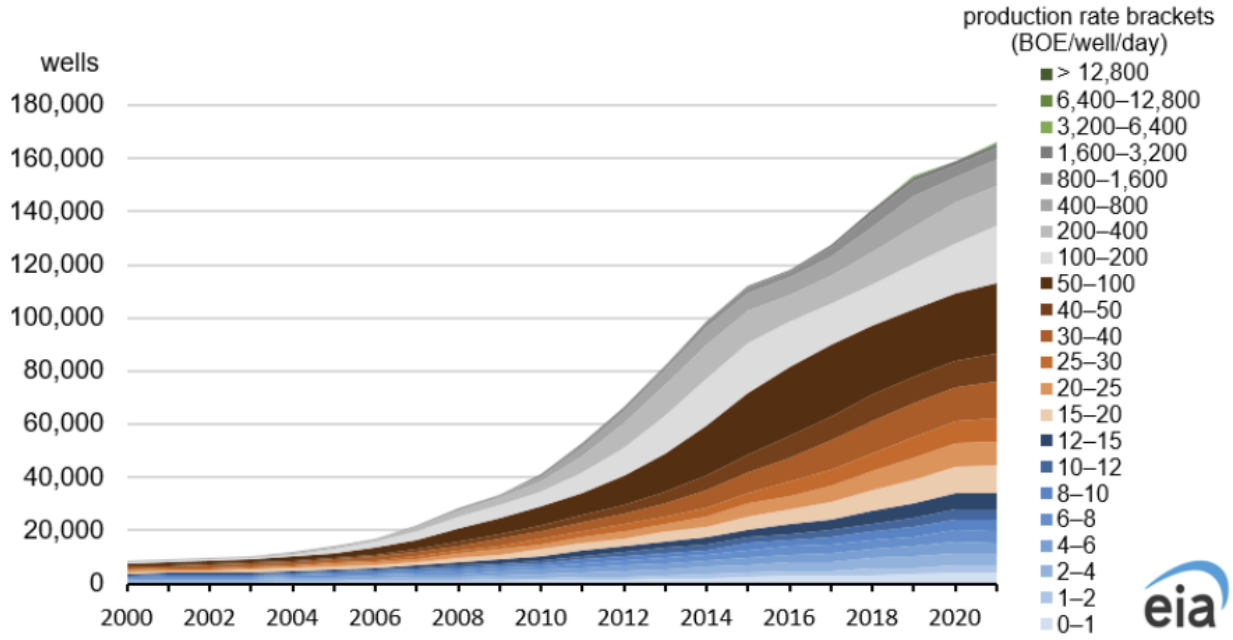

Figure 5. Lateral wells producing in the U.S. (EIA, 2022)

Therefore, the oil and gas industry is one that is simultaneously under direct scrutiny to continuously push technological boundaries while simultaneously expected to operate under the safest possible conditions (Romero et al., 2022), hence, the industry is now allocating significant resources for the development of those technologies regarding well-cementing. Recognizing its primordial role, well-cementing stands out as a fundamental element, if not the most important, in ensuring wellbore integrity, where cement acts as the main barrier between the casing and the formation, providing support and isolation for the casing, as well as preventing casing corrosion. This emphasis aligns with the importance of proper cement design, which significantly mitigates risks associated with well construction such as de-bonding, micro annulus, and poor quality of cement, as highlighted by Teodoriu et al., 2010.

A poor cementing job can lead to significant problems jeopardizing the feasibility of the project due to the cost overruns that will be incurred in remedial or squeeze operations, in addition to the economic losses due to non-productive time due to the problems generated by the inadequately executed cementing, or in the worst case, the total ordering of the well that would lead to considerable economic losses endangering the economic stability of the companies involved in such operations.

Hence, an understanding of the mechanical and thermal properties of cement, which is one of the main components of wellbore construction, and how the use of different additives such as geopolymers like class F fly ash, and sodium hydroxide will affect the behavior of the cement is of paramount importance for the industry for the assurance of the different operations that are going to be done through the use of the well that is going to be constructed or intervene.

1.2 Objectives.

1.2.1 General Objective.

The main objective of this study encompasses a comprehensive evaluation of the compressive strength achieved by different class G cement composites cured under high temperatures with the aim of contrasting with the same composites that have been cured at room temperature conditions. Additionally, an evaluation of the thermal properties of some of the class G cement composites cured at room temperature previously evaluated is also conducted. Both studies were conducted for a period of 28 days.

1.2.1 Specific Objectives.

- Conduct a comprehensive literature review focused on well cementing and well integrity, along with an overview of cement and fly ash in the oil and gas industry.

- Elaborate a methodology aligned with API 10B for the conduction of laboratory testing pertaining to the compressive strength of the different class G cement composites, likewise for the measurement of the thermal properties.
- Conduct laboratory testing of the different class G composites in order to assess both their respective thermal properties and their compressive strength.
- Analyze the change in the compressive strength of the different class G cement composites by the addition and variation of the percentage by weight of class F fly ash cured at room and high temperature. Likewise, the analysis of the compressive strength for the composites cured at high temperature that have an addition of sodium hydroxide.
- Analyze the change in the thermal properties of the different class G cement composites by the addition and variation of the percentage by weight of class F fly ash cured at room temperature.
- Compare the results obtained through laboratory testing to highlight the change of the compressive strength by the addition of class F fly ash and sodium hydroxide to class G.
- Compare the results obtained through laboratory testing to highlight the change of thermal properties by the addition of class F fly ash to class G cement.

1.3 Scope of work.

The scope of this research aims for experimental testing and analysis of the compressive strength of neat class G cement and class G cement composites with different percentages of fly ash, at both room temperature and high temperature, and class G cement with fly ash with the addition of sodium hydroxide at high temperature. Similarly, for the experimental testing and analysis of thermal properties of neat class G cement and class G cement composites with the addition of fly ash at different percentages cured at room temperature.

2 Literature review.

2.1 Well Integrity.

Nowadays, well integrity is one of the main challenges across different industries, such as the oil and gas industry, and the generation of electricity through geothermal wells, that operators are facing due to the nature and complexity of the operation that is aiming to connect the surface with the targeted zone, by drilling the well, running casing and finally the pumping of cement. Therefore, well integrity must be ensured in every operation that a well will face during its existence, starting from drilling activities, well testing, completion, workover, production, and abandonment of the well, among others.

According to the Norsok standard D-010 "well integrity refers to implementing technical, operational, and organizational measures to minimize the risk of an uncontrolled release of formation fluids during the lifespan of a well" (Norsok, 2013). Another definition of well integrity given by the American Petroleum Institute is "a state or characteristic of a well in which its mechanical integrity has competent barriers to prevent the unintentional flow of fluids that can be liquid and/or gas from one geological formation to another or to the surface"(American Petroleum Institute, 2016). Likewise, the general concept of well integrity according to the UK Oil and Gas Industry Association, is "the general activities, processes, and barriers used during the different operations with the aim of reducing the hazard of unrestrained release of fluids throughout the life of the well" (UK oil and Gas Industry Association, 2019).

Well Integrity failure is a complex problem driven by various factors, like environmental elements like geographic positioning, subsurface geology, pressure, and temperature, as well as human factors like engineering approaches and regulatory practices (Cahill et al., 2019; Sandl et al., 2021; Trudel et al., 2019).

Those problems previously mentioned have a fundamental role in the degradation of the well barriers, such as the tubulars (casing) and cement, along with the lack of understanding of the role of the barriers that are used in the well, and how the environmental factors like the temperature affect the performance of these.

According to SLB for drilling operations, the casing is a pipe with a large diameter that is positioned into an open hole to be cemented in place, meeting the specification of withstanding diverse loads, such as burst, collapse, and tensile failure and harsh conditions. The aim of the casing is to provide zonal isolation, due to a wide variety of reasons like the protection of formation with the presence of fresh water, isolation of zones with different pressure gradients, and lost return zones, among others (SLB, 2023). On the other hand, SLB has defined casing for completion operations, as a steel pipe that has been cemented in place during the drilling and construction process of stabilizing the wellbore being a major structural component serving as an isolation to prevent crossflow of formation fluids, also prevents the wall of the formation from caving into the wellbore, and providing a way of keeping control of pressure and formation fluids while the well is drilled, allowing to set up a blowout preventer in place (SLB, 2023).

2.2 Well cementing.

There exist two main operations when the operation of well cementing is done. One of those operations is known as primary cementing, which is a fundamental phase involving the placement of the cement slurry into the annulus, which is the space between the formation and the casing. On the other hand, secondary cementing or remedial cementing encompassing squeeze and plug, this operation aims to repair and correct problems due to poor quality primary cementing improving the overall integrity of the wellbore, also remedial cementing is used for an eventual abandonment of the well. Primary cementing is an important step in the well construction process.

The cement pumped to the annulus creates a hydraulic barrier that prevents the fluid connection between producing zones in the borehole and prevents fluids from escaping to the surface (Romero, 2020). This cement secures and supports the casing string while also protecting the steel casing from corrosion caused by formation fluids (Erik B, 2012). Loss of zonal isolation can result in costly well repairs, endangering personnel, and equipment, causing significant operational difficulties and massive environmental issues, and, in the worst-case scenario, total well loss (Bois et al., 2011).

2.3 Portland cement.

Cement stands as one of the most important materials all around the world, finding extensive use across various engineering projects. Additionally, it plays a vital role in the oil and gas, and geothermal industry by securely cementing casing in a well (Abid, Srivastava, et al., 2023). Portland cement is a complex material created from two simple and plentiful materials: limestone and clay (or shale). To generate a raw meal with a precise chemical composition, very exact proportions of these two fundamental elements must be blended with some extras. The cost of producing Portland cement is strongly related to the cost of the fuel necessary to generate a kiln temperature high enough to allow the many chemical processes that change raw meal into clinker to occur (Aïtcin, 2016).

2.3.1 Types of Cement according to the API.

Cement for the oil and gas industry has significant differences from its counterparts used for the construction of buildings, infrastructures, and roads. Usually, the cement used for the industries previously mentioned does not face the same hostile conditions as the one used in the oil and gas industry which faces high pressures and high temperatures, as well as has to withstand brines, acidic environments, and more.

The American Petroleum Institute has classified well cement in six different classes, which are class A, B, C, D, G, and H, that are also classified into three different grades: ordinary (O), moderate sulfate resistant (MSR), and high sulfate resistant (HSR) (American Petroleum Institute, 2010).

- Class A: “This class of cement is intended to be used when special properties are not required, it can be found in grade O cement, and it can be used for a depth of a maximum of 6000 ft and temperatures up to 170 °F.”(Renpu, 2011).
- Class B: “This class of cement is intended to be used when conditions require moderate or high sulfate resistance, hence is available in grade MSR or HSR and it can be used for a depth of a maximum of 6000 ft and temperatures up to 170 °F.” (Renpu, 2011).
- Class C: “This class of cement is intended to be used when conditions require high early strength, it is available in grade O, MSR, and HSR and it can be used for a depth of a maximum of 6000 ft and temperatures up to 170 °F.” (Renpu, 2011).
- Class D: “This class of cement is intended to be used when conditions require resistance to moderately high temperatures. Available in grade MSR and HSR, it can be used for a depth of a maximum of 6000 ft and temperatures up to 230 °F.” (Renpu, 2011).
- Class G: “This class of cement is intended to be used as the standard for basic well cementing. Available in grade MSR and HSR, it can be used for a depth of a maximum of 8000 ft and a wide variety of temperatures.” (Renpu, 2011).
- Class H: “This class of cement is intended to be used as the standard for basic well cementing. Available in grade MSR and HSR, it can be used for a depth of a maximum of 8000 ft and a wide variety of temperatures.” (Renpu, 2011).

2.3.2 Cement Additives.

The use of chemical additives in the oil and gas industry can modify the rate of hydration that occurs when water and cement are mixed. Those additives are chemicals or materials that are blended into the neat cement slurries in order to change their performance to achieve the needs of the operation (Broni-Bediako, 2016). Commonly used chemical additives in oil and cementing procedures encompass accelerators, retarders, extenders, additives for loss circulation, and dispersants, among others (Roshan, 2010).

- Accelerators: chemical additives used to speed up the thickening time of the cement, increasing the early development of the compressive strength. Those accelerators can be calcium chloride, and sodium chloride among others.
- Retarders: It is a chemical additive that is used to delay cement hydration; hence the development of the compressive strength is much slower. Some of the retarders are lignosulfonate, cellulose derivatives, and hydroxycarboxylic acids.
- Extenders: Material or chemical used to lower the density of the mixture, hence the hydrostatic pressure of the same is going to be lower. Bentonite and sodium silicate are the common extenders that are used in the oil and gas industry.
- Heavy-weight agents: The requirement for an additive to be considered a heavy-weight agent is to have a greater specific gravity than the cement, even particle size, and low water requirements in order to restrain high formation pressure. Hematite and ilmenite are commonly used for this purpose.
- Fluid loss additive: commonly used to reduce the rate at which water from the cement is absorbed by the formation due to differential pressure. The most common additive for fluid loss is hydroxyethyl cellulose.

- Dispersants: This additive is used to improve the flow properties of cement slurries. It is particularly used to compensate for high viscosity and the tendency to gel of some cement slurries.

2.3.3 Chemical composition of Portland cement.

Portland cement is widely used in the oil and gas industry, for the operation of well cementation, as well as for sealing the injection sites in the wells chosen for carbon sequestration. (Abid, 2018). The Blaine-specific surface area of the Portland cement is 280-340 m2 /kg (Kurdowski, 2014). Functions and compositions are summarized in **Table 1**.

Compound	Cement Chemist Notation	Content (wt %)	Function
Tricalcium Silicate $(CaO)_3 . SiO_2$	C_3S	58	Enhances the strength and develops early strength
Dicalcium Silicate $(CaO)_2 . SiO_2$	C_2S	19	Hydrates slowly, Strength generated over time
Tricalcium Aluminate $(CaO)_3 . Al_2O_3$	C_3A	2	Promotes rapid hydration, affects thickening time and initial setting of the cement
Tetracalcium Aluminoferrite $(CaO)_4 . Al_2O_3 . Fe_2O_3$	C_3AF	11	Responsible for slow hydration

Table 1. Specific functions and composition of Portland cement (Charrier., 1985)

2.3.4 Hydration of cement.

The reason Portland cement is known as hydraulic cement is that its strength is built due to the chemical reactions that happen between the cement and the water. The process that has been described before is known as hydration. This process provides hardening, solidification, and rigidity to the cement (Abid, 2018),

2.3.5 Hydration of silicates.

80% of the cement composition is silicates, making silicates the predominant phase that is present in Portland cement (Nelson, 1990). Of that 80%, about 20% of the Portland cement consists of C2S, however, around 70% is C3S. The interaction between silicate and water is shown below ((Sidney Mindess, 2003) (Michael S. Mamlouk, 2011).

$$2C3S + 7H \rightarrow C3S2H8 + 3CH \qquad \textit{Equation 1}$$

$$2C2S + 7H \rightarrow C3S2H8 + CH \qquad \textit{Equation 2}$$

Calcium Silicate Hydrate (C-S-H) and Calcium Hydroxide (CH), often known as Portlandite, are formed in both processes. C3S, on the other hand, produces more C-S-H than C2S. Because the hydration rate of C3S is significantly faster than that of C2S, the early strength in the cement is caused by its hydration. C2S strength, on the other hand, comes later in the hydration process (Abid, 2018).

2.3.6 Hydration of Aluminate Phase.

C3A has a lower abundance than the silicate phase but has a stronger influence on the rheology and early strength development of the cement. C4AF hydration at a comparable pace as C3A, but at a considerably slower rate (Nelson, 1990). C3A interacts with gypsum (CSH2) and water in the first phase to produce ettringite (C6AS3H32) as shown below:

$$C3A + 3CSH2 + 26H \rightarrow C6AS3H32 \qquad \textit{Equation 3}$$

The ettringite's stability is determined by the availability of gypsum. It is important to note that ettringite does not participate in the cement's strength development. When all the gypsums have been consumed, the ettringite begins to react with any residual C3A to generate monosulphate aluminate hydrate crystals, which are denoted as (Abid, 2018)

$$2C3A + C6AS3H32 + 22H \rightarrow 3C4ASH18 \qquad \textit{Equation 4}$$

In the sulfate-deficient solution, the monosulphate crystals are stable. However, in the presence of sulfate, these monosulphate crystals may revert to ettringite. The ettringite crystal is two and a half times larger than the monosulphate crystal and is responsible for cement cracking in the presence of sulfate (Sidney Mindess, 2003) (Michael S. Mamlouk, 2011).

2.3.7 Temperature on cement setting.

An important consideration in the design of a cement composite and any other related cementing operation is the correct determination of the reservoir temperature or downhole operating temperature to which the cement composite is going to be subjected. This factor comes into play for the reason that temperature fluctuation has a significant impact on the cement composite behavior and performance this is due to the initial exothermic reaction that the cement has within the first 24 to 36 hours, and the endothermic process that cement goes through after that initial time (Batista da Silva et al., 2018; Luke, 2004; Vu et al., 2012; W. C. Wang, 2017).

High temperatures are usually found in deep wells, in which the hydrated products of the cement are projected to experience substantial changes in the mechanical properties, shortening the setting time and achieving a higher compressive strength, which also leads to substantial chemical and microstructural changes in the cement composite (Bahafid et al., 2018; Batista da Silva et al., 2018; Karim et al., 2018; Mahmoud & Elkatatny, 2019; Rincon, Teodoriu, et al., 2022).

2.4 Fly ash.

A waste product produced when coal is burned in coal-fired thermal power plants is called fly ash. About 750 million tons of fly ash are produced annually as a byproduct from thermal power generation plants, creating a significant disposal issue. Fly ash is an essential supply of engineering materials, but it has not been utilized to its full potential (Kabir et al., 2016).

Therefore, the characteristics of fly ash rely on the kind of technology employed in its manufacturing. Before the flue gases are expelled, fly ash is formed and liberated using two different types of boilers. There are two types of boilers: fluidized bed boilers and typical pulverized coal boilers (Kar, 2022). For the time being, the primary subjects of conversation are coal and the various varieties of coal, both of which are essential in establishing the characteristics of fly ash (Matsunaga et al., 2002).

The coal-fired thermal power plant generates 60% to 88% of the fly ash, which is collected using particle control pollution equipment such as electrostatic precipitators. This fly ash is produced by burning coal at high temperatures of about 1200°C to 1700 °C, and it is constituted of several organic and inorganic components. Due to their challenging composition, varied particle size and shape, fine size, and composition fly ash identification, specification, characterization, and usage are challenging procedures (Kar, 2022).

2.4.1 Chemical composition of fly ash.

The main difference between geopolymers and cement structurally speaking is determined by the chemical bond that is present in the material. While cement is built on hydration and ionic bonding, geopolymers are made of 3D covalent bonds as a result of polycondensation of inorganic aluminosilicate solution (Humairah et al., 2021). Additionally, the chemical composition and activation of the compounds present in the geopolymers account for the majority of the performance variation (Romero et al., 2022). Geopolymers are created by the alkaline activation of aluminosilicates-based materials like fly ash, different as cement which is based on hydration (Salehi et al., 2016). Nonetheless, depending on the kind of coal used in the combustion as well as the combustion process employed, the chemical composition of fly ash might vary from batch to batch (Kar, 2022) as seen in **Table 2**.

Component (mass %)	Bituminous	Subbituminous	Anthracite	Lignite
Al_2O_3	5–35	20–30	25.1–29.2	10–25
MgO	0–5	1–6	0.7–0.9	3–10
Fe_2O_3	10–40	4–10	3.8–4.7	4–15
SiO_2	20–60	40–60	43.5–47.3	15–5
CaO	1–12	5–30	0.5–0.9	15–40
Na_2O	0–4	0–2	0.2–0.3	0–6
K_2O	0–3	0–4	3.3–3.9	0–4
SO_3	0–4	0–2	–	0–10
TiO_2	0.5	1.1–1.2	1.5–1.6	0.23–1.68
P_2O_5	0.02	0.3–0.5	0.2	–
MnO	0.02	0.1	0.1	0.04–0.21
S	0.08–0.67	0.7	0.1	–
Loss on ignition	0–15	1.8–2.7	8.2	0–5

Table 2. Composition of fly ash obtained from different coals (Gollakota et al., 2019).

Furthermore, the chemical composition of fly ash exhibits variability depending on the final utilization, class C fly ash and class F fly ash. **Table 3** shows a significant variation of oxide elements percentages present in it.

Element oxides	Class C Percentage	Class F
CaO	15.1–54.8	0.50–14.0
SiO_2	11.8–46.4	37.0–62.1
Al_2O_3	2.6–20.5	16.6–35.6
Fe_2O_3	1.4–15.6	2.6–21.2
MgO	0.1–6.7	0.3–5.2
K_2O	0.3–9.3	0.1–4.1
Na_2O	0.2–2.8	0.1–3.6
SO_3	1.4–12.9	0.02–4.7
P_2O_5	0.2–0.4	0.1–1.7
TiO_2	0.6–1.0	0.5–2.6
MnO	0.03–0.2	0.03–0.1
Loss on ignition (LOI) (%)	0.3–11.7	0.3–32.8

Table 3. Element oxides are present in Class C and Class F fly ash (Hemalatha and Ramaswamy, 2017).

However, while heat works as a catalyst for the geopolymerization of fly ash, some researchers have confirmed that temperatures beyond 100 °C cause the compressive strength of the material to decrease. This decrease is related to the significant moisture loss that caused the specimens to crack (Okoye et al., 2015).

2.4.2 Class F fly ash.

The American Society for Testing and Materials commonly divides fly ash into two classes: Class C fly ash (high calcium) and Class F fly ash (low calcium) (ASTM) (T. Hemalatha, 2022) Due to its widespread availability and additional technical benefits including decreased heat of hydration, bleeding, segregation, permeability, enhanced sulfate resistance, acid resistance, etc., low calcium fly ash is utilized extensively. Nevertheless, there have also been observed drawbacks with low calcium fly ash in concrete, such as poorer carbonation resistance and higher water absorption (Rashad, 2015).

2.4.3 Activation of Fly ash.

There are two primary processes used in chemical activation approaches. Those chemical activations are sulfate activation and alkali activation (Lee et al., 2003; Poon et al., 2001). Different types of alkali activators are used for the activation of FA, in general, calcium hydroxide (Ca (OH)2) or sodium hydroxide (NaOH), or any other oxide is used to increase the alkalinity. The increase in alkalinity corrodes the densified outer glassy layer exposing the active core for a faster reaction (T. Hemalatha, 2022).

2.5 Thermal properties.

When heat is applied to solids, liquids, or gases, a wide range of reactions occur depending on the material. These responses are referred to as thermal properties. These reactions result in changes in different physical or chemical variables, temperature increases, transformational phase transitions, length or volume changes, and the activation of chemical processes through catalysis. The complicated interaction between the thermal dynamics of a substance and its structural and compositional properties is highlighted by the complexity of the reactions, which leads to a rich tapestry of behaviors seen in many states of matter (Buck & Rudtsch, 2011).

2.5.1 Conductivity.

The ability of a material to allow the transfer or conduction of heat is characterized by its thermal conductivity, denoted by the letters k, λ, or κ. Another definition refers to the amount of heat that goes through a plate with a particular material and thickness, its faces having a temperature differential of one unit, across a unit area in a unit of time. Thermal conductivity mostly results through molecular motion and contact; there is little to no movement of the solid's mass. A temperature gradient causes heat to go from areas with high temperatures and high

molecule energies to those with low temperatures and low molecular energies (Thermtest Instrument, 2019).

2.5.2 Diffusivity.

Thermal diffusivity is a parameter that measures the temperature change that occurs in a unit volume of a material as a result of a certain quantity of heat passing through a unit area of a layer with a unit thickness and faces that exhibit a unit temperature difference. It is typically denoted by α. The relationship between thermal diffusivity and the rate at which heat spreads during temporal temperature variations reveals the pace at which thermal changes move through a material (Salazar, 2003).

2.5.3 Heat capacity.

The fundamental thermodynamic parameter of heat capacity, also referred to as total heat capacity or C, defines how much heat is required to change the temperature of a substance by one Kelvin. It essentially describes the thermal responsiveness to temperature changes of a substance, providing a useful statistic to understand how well a substance releases or absorbs heat. It is measured in joules per Kelvin (J/K) units (B. X. Wang et al., 2010).

2.5.4 Effusivity.

The ability of a material to facilitate the transmission of thermal energy to the surrounding environment is shown by its thermal effusivity, also known as thermal inertia. The calculation of the square root of the product of thermal conductivity and heat capacity gives this important quantity, that includes the thermal properties of the material, particularly those related to the effective transfer of thermal energy (Cottrill et al., 2018).

3 Methodology.

3.1 Materials and Methods.

This section provides a comprehensive overview of the experimental methodology, describing the materials employed, the methodology for sample preparation, and the specific equipment utilized for conducting the sample test throughout the execution of the research.

3.2 Sample preparation.

The initial phase in sample preparation involves precise measurement of material weights utilizing a digital balance as illustrated in **Figure 6.**

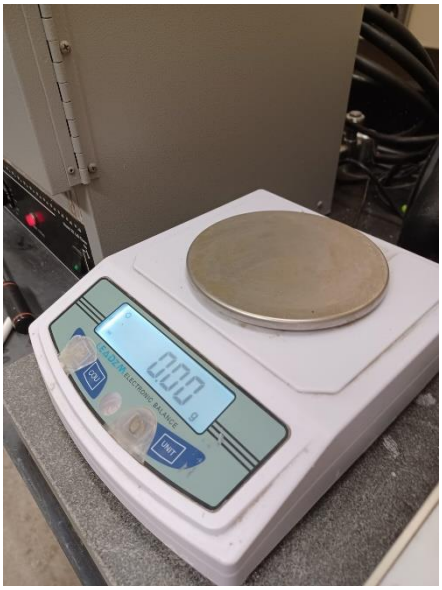

Figure 6. Digital balance.

In the initial set of experiments, a precise weighing of the materials was done, starting with 792 grams of class G cement and 348 grams of distilled water, which is going to produce 600 ml of cement slurry, establishing the control samples for this research. Subsequently, for the second set of experiments involving the addition of fly ash to the original recipe at different percentages (10% - 79.2 grams, 20% - 158.4 grams, and 30% - 237.6 grams), the respective amounts of fly ash

were weighed and incorporated into the mixture. Finally, for the last set of experiments, sodium hydroxide (NaOH) was added to the mixture at half of the weight of the fly ash, ergo 39.6 grams for 10%, 79.2 grams for 20%, and 118.8 grams for 30% fly ash, refer to **Table 4** for easier understanding.

Sample	Materials			
	Distilled water (grams)	class G cement (grams)	Fly ash (grams)	Sodium hydroxide (grams)
Class G	348	792	-	-
Class G + 10% FA	348	792	79.2	-
Class G + 20% FA	348	792	158.4	-
Class G + 30% FA	348	792	237.6	-
Class G + 10% FA + NaOH	348	792	79.2	39.6
Class G + 20% FA + NaOH	348	792	158.4	79.2
Class G + 30% FA + NaOH	348	792	237.6	118.8

Table 4. Samples and recipes.

Secondly, once all the materials have been measured, the handling diverges based on the experiment set. In the first set of samples, the material remains in its original state. For the second set of samples, a manual mixing process is initiated, where the class G cement and fly ash are blended by hand until homogeneity. Finally, in the third set of samples, an additional step is introduced. Here the dry materials, class G cement, and fly ash go through the same blending process, followed by the addition of sodium hydroxide to the distilled water. Once all the respective procedures are done the wet material is poured into the mixer **Figure 7**.

Figure 7. Ofite high shear mixer.

Subsequently, the mixer is promptly initiated, and within the initial 15 seconds, the neat class G cement or the pre-blended mixture is carefully added into the mixer set at a shear rate of 4000 RPMs. Just before the laps of the 15 seconds, the top of the lid is closed, for the following high shear mixing at 12000 RPMs that last 35 seconds. Once the stipulated mixing time concludes, the cement slurry is poured into the metallic molds that were previously greased **Figure 8**. These molds, in adherence to API-10B2 guidelines corroborated by Rincon (Rincon, Abid, et al., 2022) are designed to create three 2" x 2" cubes. This decision is in line with Rincon's findings, which claim that cylindrical samples do not accurately represent the mechanical properties of the cement nor efficiently correlate with UPV-UCS (Ultrasonic Pulse Velocity - Unconfined Compressive Strength) measurements.

Figure 8. Metallic molds.

Following the molding, the cement cubes are carefully immersed in water baths, that can be at room temperature or maintained at an elevated temperature of 75°C, as depicted in **Figure 9.** The submersion of the samples initiates the curing process, allowing the samples to garden adequately within the molds. The samples are removed from the molds once are hard enough, and then are placed again in their respective water baths to continue the curing process.

Figure 9. Class G + 20% FA being cured at high temperature.

3.3 Compressive strength measurement.

A destructive test is performed, using a compression testing machine CM-2500 **Figure 10**, manufactured, and calibrated by Test Mark Industries, to determine the unconfined compressive strength of the different cement composites used in this study. According to the manufacturer, the

CM-2500 has a precision of ± 0.5% the machine applies a uniaxial load to the cement composite sample maintaining a controlled rate of 72 kN ± 7kN per minute, measuring the force that was required to deform the sample plastically or permanently.

The unconfined compressive strength then is calculated by dividing the maximum force that was applied by the surface area of the sample. The results obtained then are reported to the nearest 0.3 MPa and then the average is calculated out of three samples that were previously made from the same pour as long as it is possible, according to API RP 10B-2.

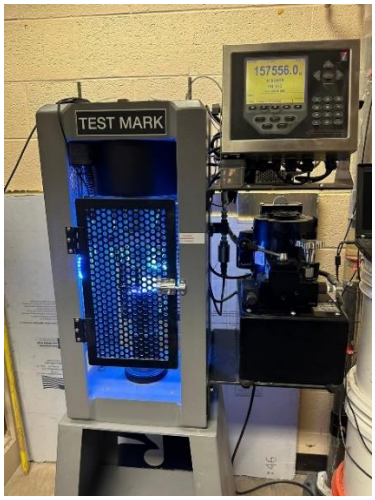

Figure 10. Test Mark CM-2500.

3.4 Thermal properties measurement.

The first instrument used for measuring the value of the thermal conductivity, diffusivity, heat capacity, and effusivity was the Keithley 2400 meter with transient plane source (TPS)-3, as depicted in the right portion of **Figure**. Then, the next equipment utilized for measuring just thermal conductivity along with Keithley 2400 meter with transient plane source (TPS)-3 consisted of a Thermtest Portable Measurement Platform −2 (MP 2) having a probe of 50mm, showcased in

the left section of **Figure 11**.

The Thermtest Portable Measurement Platform −2 (MP 2) works on the principle that uses the probe placed in the 4mm hole drilled in the sample's center to take the thermal conductivity reading. However, with the Keithley 2400 meter with TPS-3, the sensor is positioned between the samples and the reading is taken from the outer surface.

Figure 11. Keithley 2400 meter with TPS-3 (right) and Thermtest Portable Measurement Platform −2 (left).

3.5 Density measurement.

The density of the samples was obtained in an analytical way, where each dimension of the cubes designated for the measurement of the thermal properties was carefully measured to calculate the volume of the cube using **Equation 5**. It is calculated by subtracting the volume of a cylinder from the volume of the cube. The volume of the cylinder was taken in the calculation because of the hole that was drilled in the cube.

$$V = (L_1 * L_2 * L_3) - (\pi * r^2 * L_1)$$

Equation 5

Subsequently, the weight of each sample was measured using a digital balance **Figure 6**. Finally, the sample density was calculated by performing a division operation **Equation 6** between the weight and the volume previously calculated.

$$\rho = \frac{V}{W}$$

Equation 6

4 Results.

The following section will show the results obtained for the compressive strength measurements and the measurements for the thermal properties of all the different cement composites used throughout the research. All these results are going to be shown mainly through graphs showing the change of the different properties during the period of testing, as well as the mention of the main effects that the additive had on the property that was measured on the respective graph.

4.1 Compressive strength.

4.1.1 Class G.

The control samples, class G cement, were tested at room temperature, starting with an approximate compressive strength of 13 MPa on day one. Likewise, it was possible to see a steady increase in the development of the compressive strength, until the 14th day when it almost reached a stable compressive strength with minor increases until day 28 when the samples reached about 60 MPa, as seen in **Figure 12**.

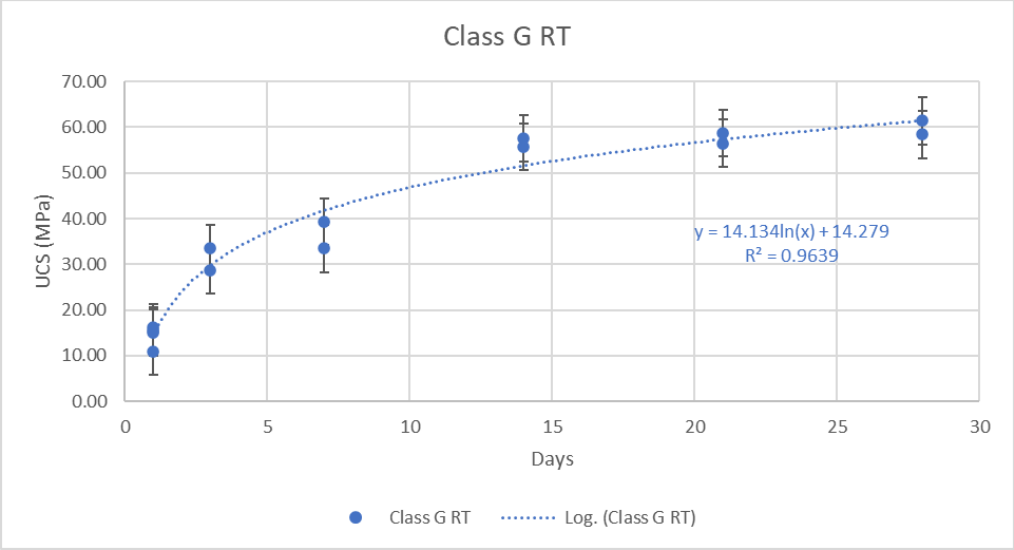

Figure 12. Class G room temperature.

Continuing with the control samples, tested at high temperatures, we see a rapid development of the compressive strength of those samples, starting around 37 MPa and then reaching stability on day 3 as seen in **Figure 13**, ending with a compressive strength of about 42 MPa.

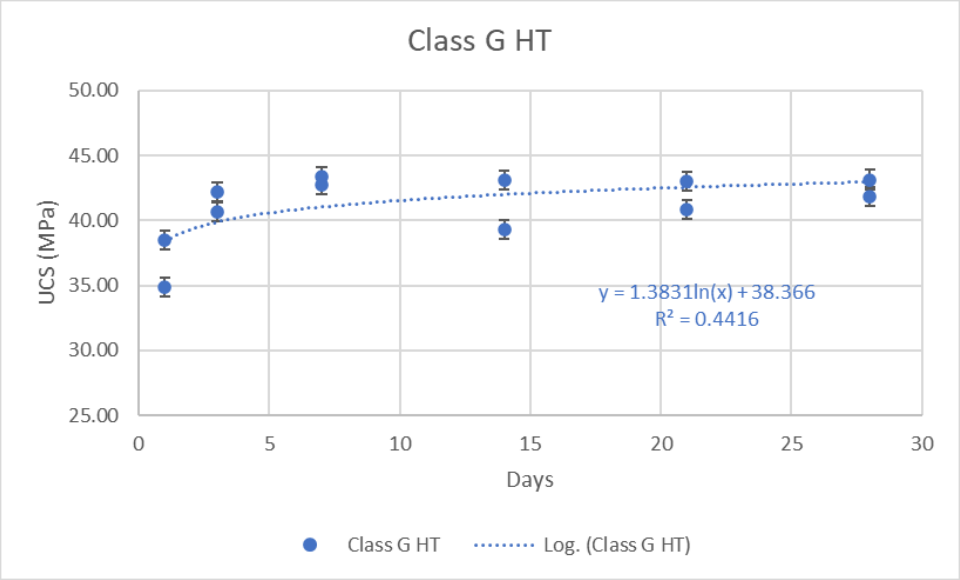

Figure 13. Class G high temperature.

Additionally, the compressive strength of the room temperature samples from day 14th to day 28th were greater than the compressive strength of the samples cured at high temperature as seen in **Figure 14** which shows the combined behavior of the neat recipes cured at different temperatures, ending up with 29% higher compressive strength on day 28th.

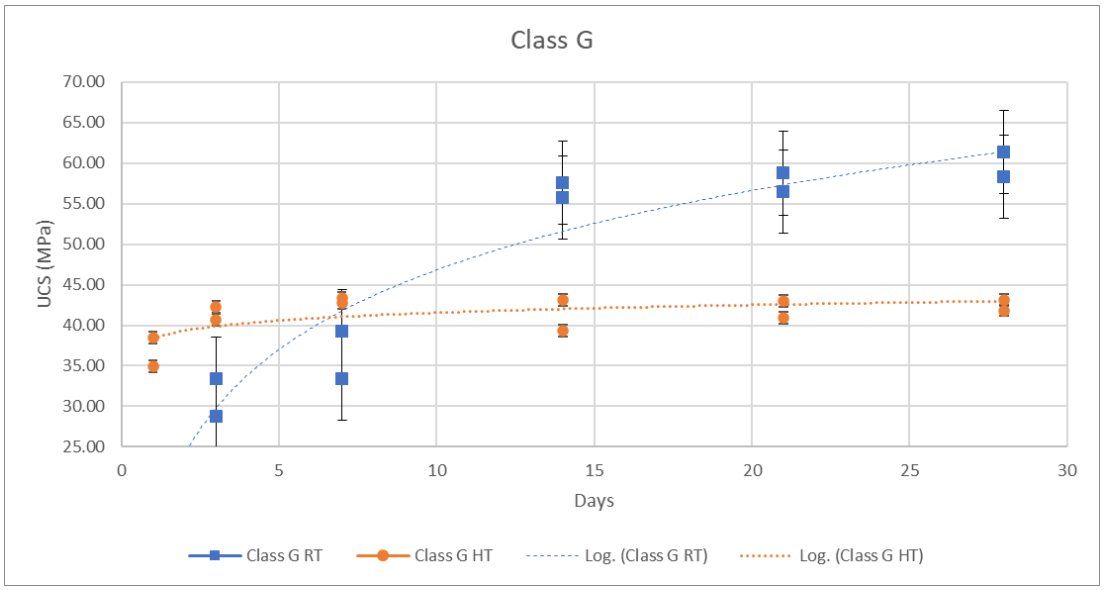

Figure 14. Class G

4.1.2 Class G + 10% fly ash.

When Fly ash is added to the mixture at 10% by weight cured at room temperature, the development of the compressive strength is gradually throughout time until day 28th reference to **Figure 15,** starting around 20 MPa on day 1 and ending up around 65 MPa by day 28th.

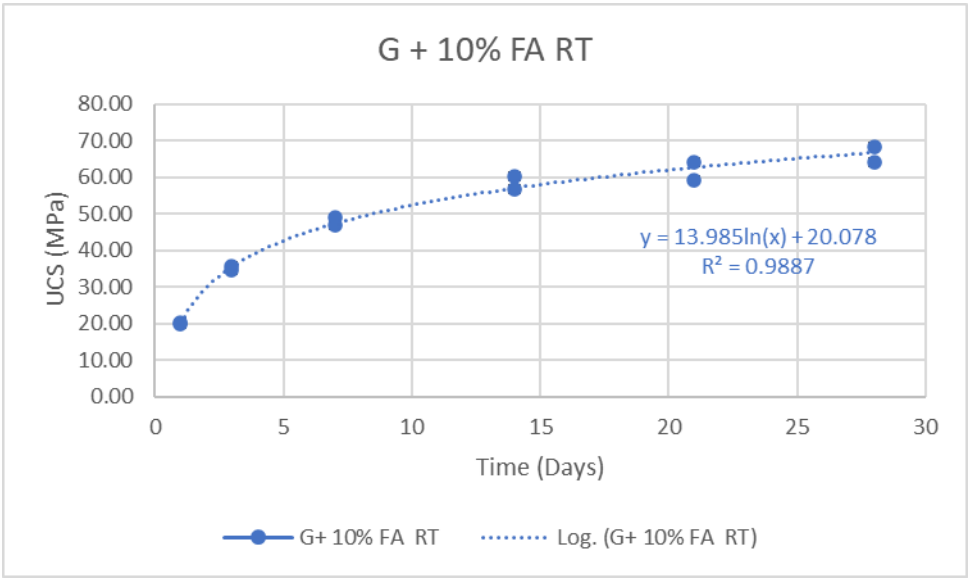

Figure 15. Class G + 10% FA room temperature.

On the other hand, when the same samples were cured at high temperatures and were tested, it was evident a faster development of the compressive strength, starting at around 44 MPa, then reaching its peak on day 21 with an average of 57.5 MPa, and finally having a decline on the compressive strength on day 28 with roughly 53 MPa as seen on **Figure 16**.

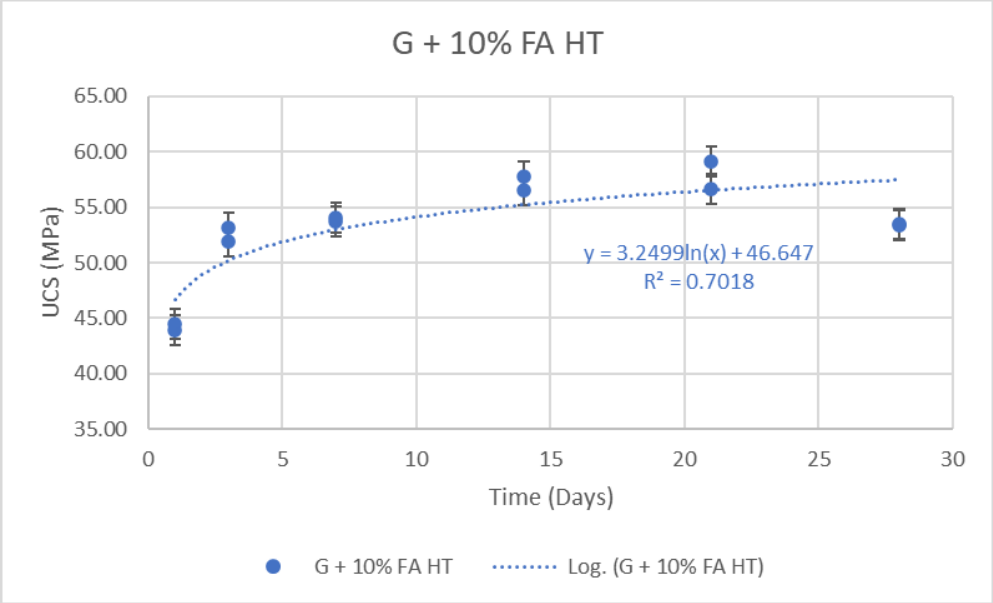

Figure 16. Class G + 10% FA high temperature.

In the beginning, the samples cured at high temperatures had a compressive strength that was twice as great as the samples cured at room temperature. However, as shown in **Figure 17,** the samples cured at room temperature eventually had a compressive strength that was greater than the samples cured at high temperatures.

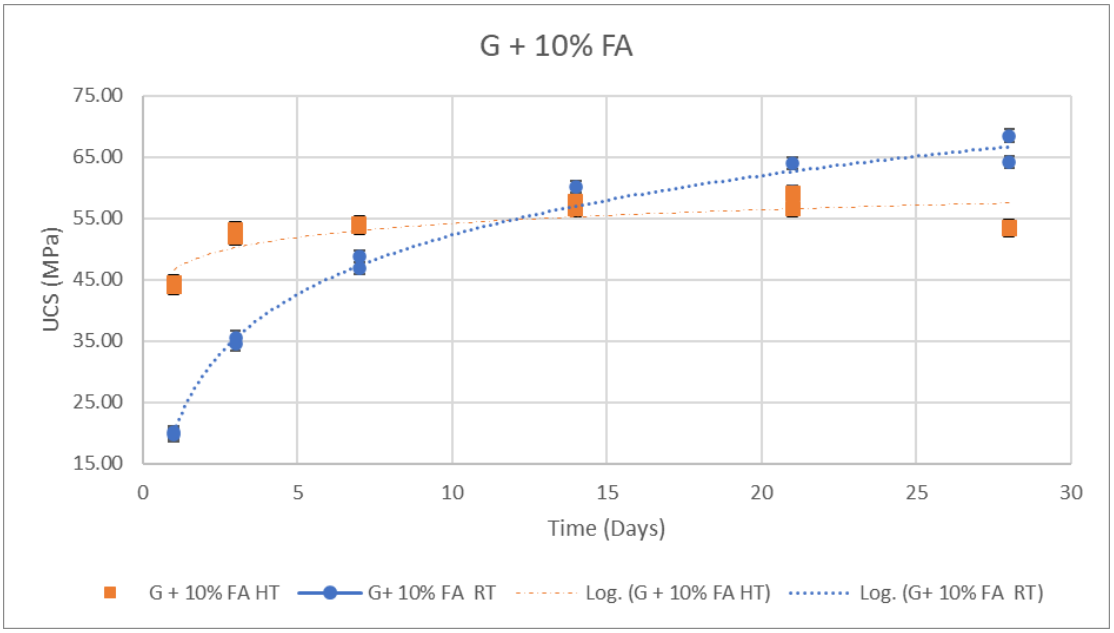

Figure 17. Class G + 10% FA.

4.1.3 Class G + 20% fly ash.

Moving on to the samples with 20% fly ash by weight added to the mixture cured at room temperature, as in the previous sample the development of the compressive strength is gradual until day 21, starting with roughly 14 MPa on day 1, reaching its peak on day 21 attaining around 61 MPa and, having a slight decrease on day 28 with roughly 59 MPa as seen on **Figure 18.**

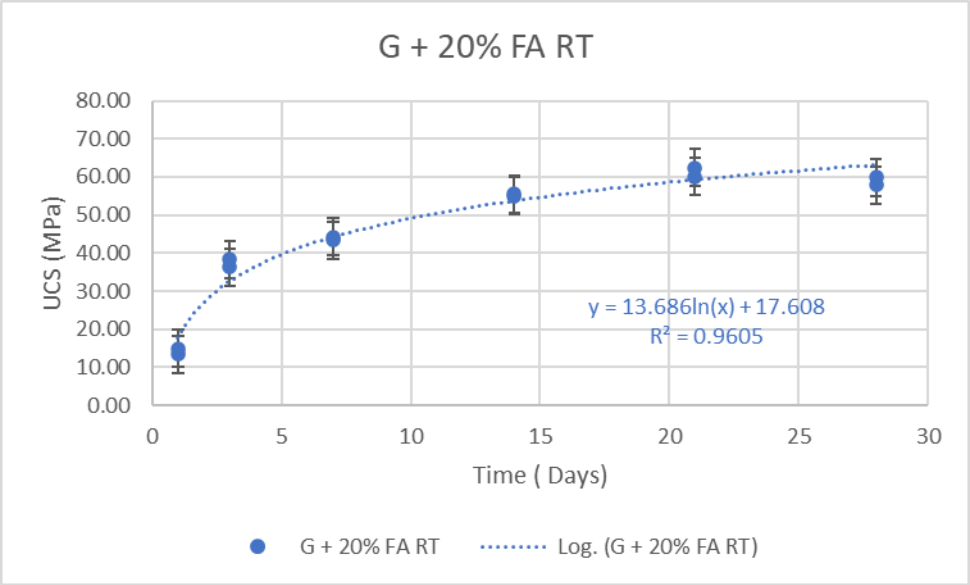

Figure 18. Class G + 20% FA room temperature.

Next, the same type of samples but cured at high temperatures were tested, having slight increases in the development of the compressive strength throughout all the tests as displayed in **Figure 19**, starting around 58 MPa on day 1 and ending up with 66 MPa on day 28.

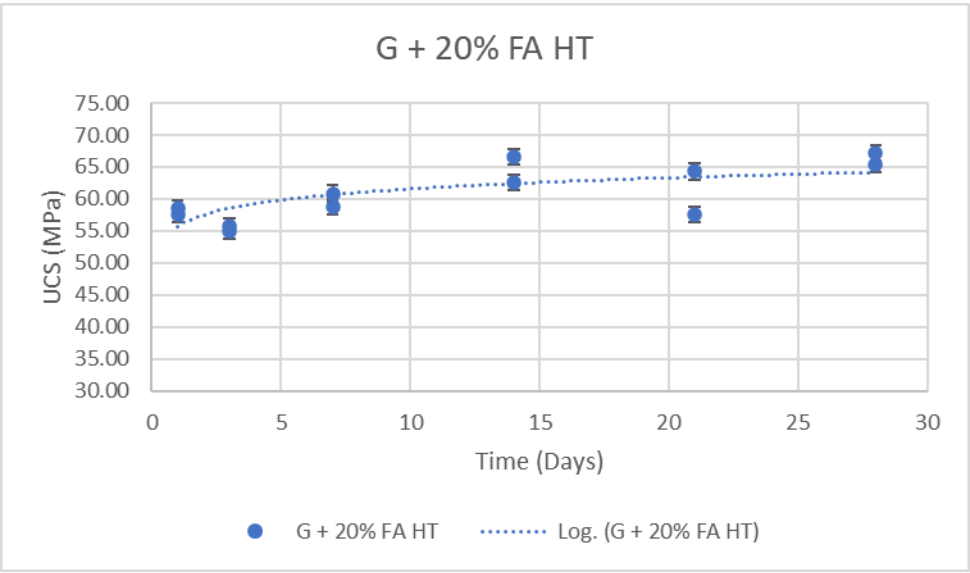

Figure 19. Class G + 20% FA high temperature.

The overall compressive strength of the samples cured at high temperature is greater than the samples cured at room temperature, likewise, the development is faster on the samples cured at high temperature as reflected in **Figure 20**, showing high values since day 1.

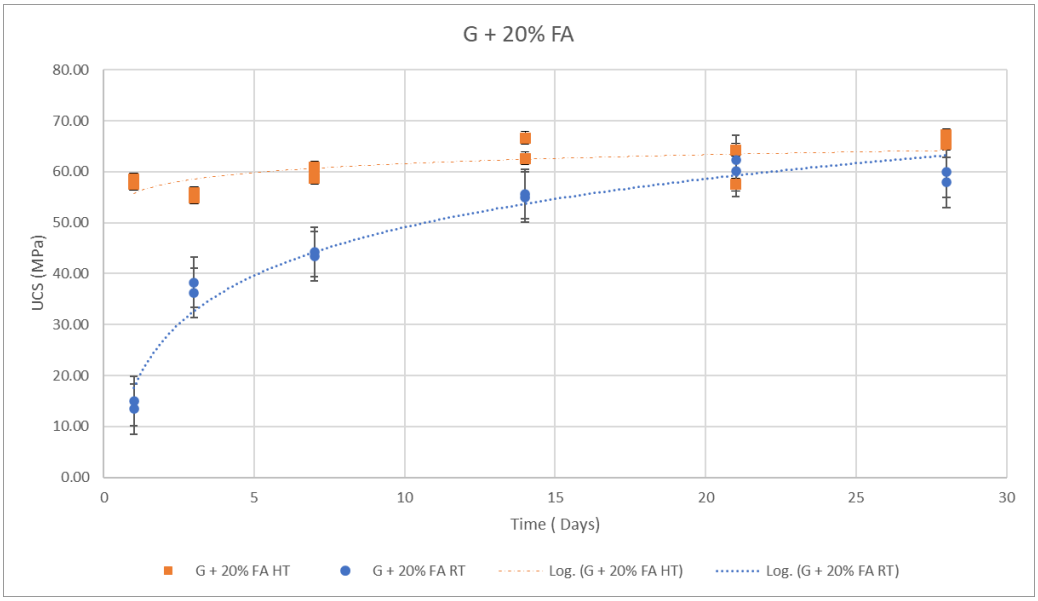

Figure 20. Class G + 20% FA

4.1.4 Class G + 30% fly ash.

Afterward, the samples mixed with 30% fly ash added by weight that were cured a room temperature were tested, once again the development of the compressive strength of these samples occurred gradually until the end of the test, starting on day one with an approximate value of 15 MPa, and ending up with around 69 MPa on day 28 as seen on **Figure 21.**

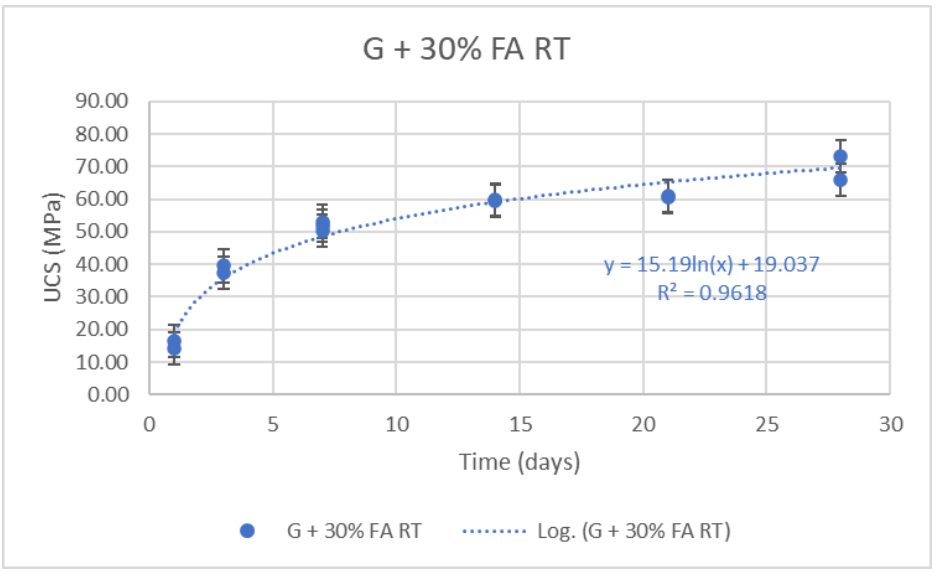

Figure 21. Class G + 30% FA room temperature.

Then, the same samples but now cured at high temperatures see **Figure 22** were tested for the same period of time, again the samples that were cured at high temperatures had a faster development of the compressive strength, departing with a tendency of around 58 MPa on day 1 and finishing up with approximately 71 MPa on day 28.

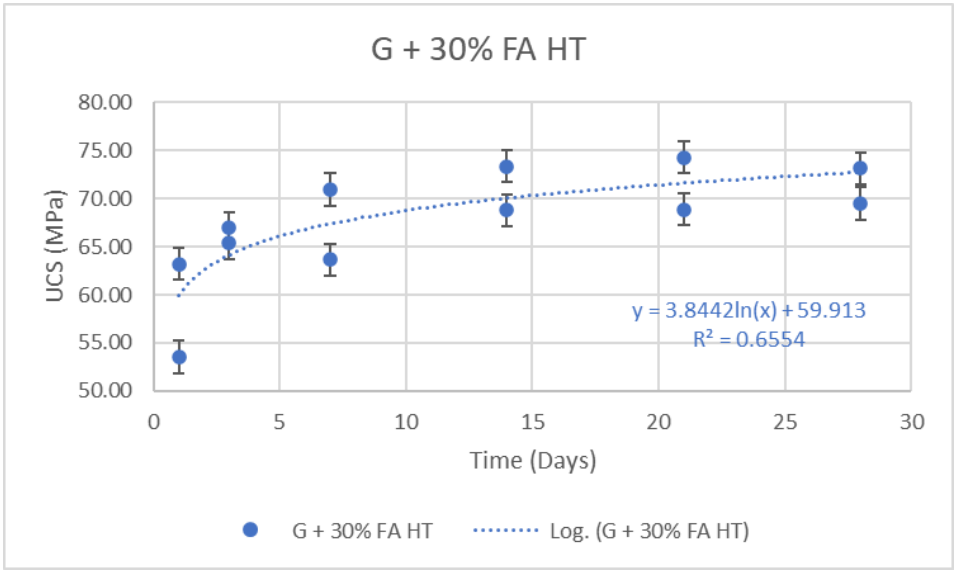

Figure 22. Class G + 30% FA high temperature.

Both samples, the ones cured at room temperature and high temperature reach a similar final compressive strength after 28 days of curing, however, the main difference between these two is initial compressive strength, where the high-temperature ones have a faster development, but this difference becomes smaller throughout time as seen in **figure 23.**

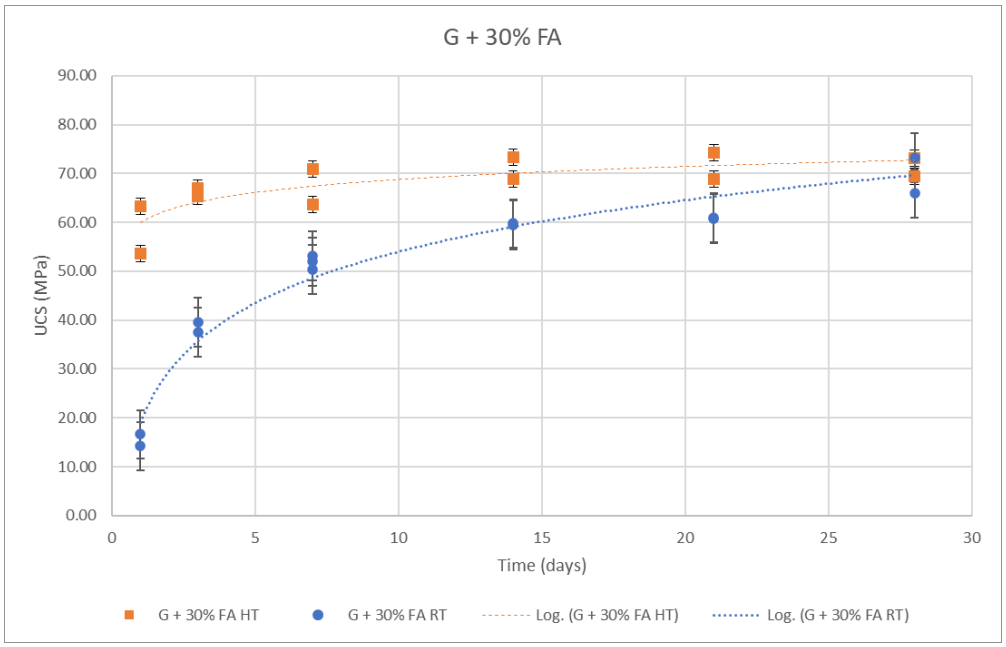

Figure 23. Class G + 30% fly ash.

4.1.5 Class G + 10% fly ash + NaOH.

Starting with the third set of experiments **Figure 24** where sodium hydroxide was added, being half of the weight of the fly ash, it is possible to see a steady development of the compressive strength, starting at about 23 MPa on day one and reaching about 25 MPa on day 28.

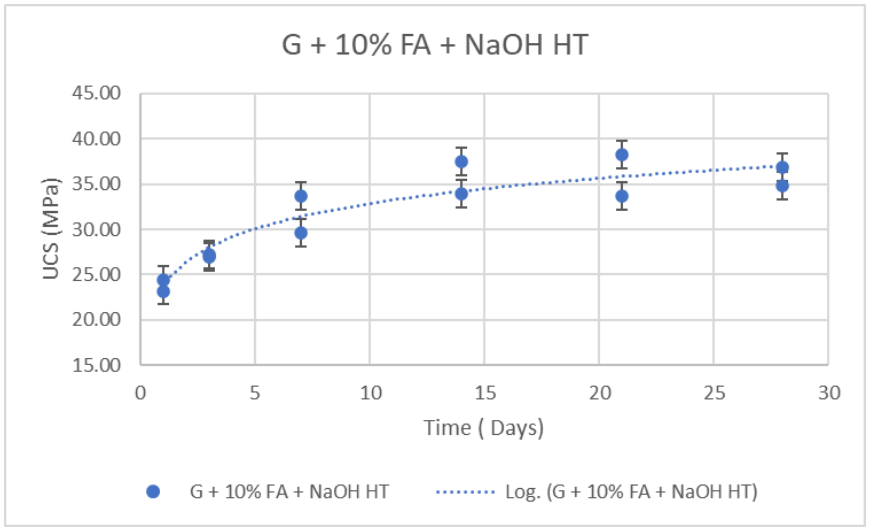

Figure 24. Class G + 10%FA + sodium hydroxide

However, when it is compared to the samples cured at high temperature without sodium hydroxide added to the mixture, it was evident that the development of the compressive was slowed during the whole duration of the test **Figure 25**, where the maximum compressive strength achieved by the samples with sodium hydroxide was about half of the ones without it.

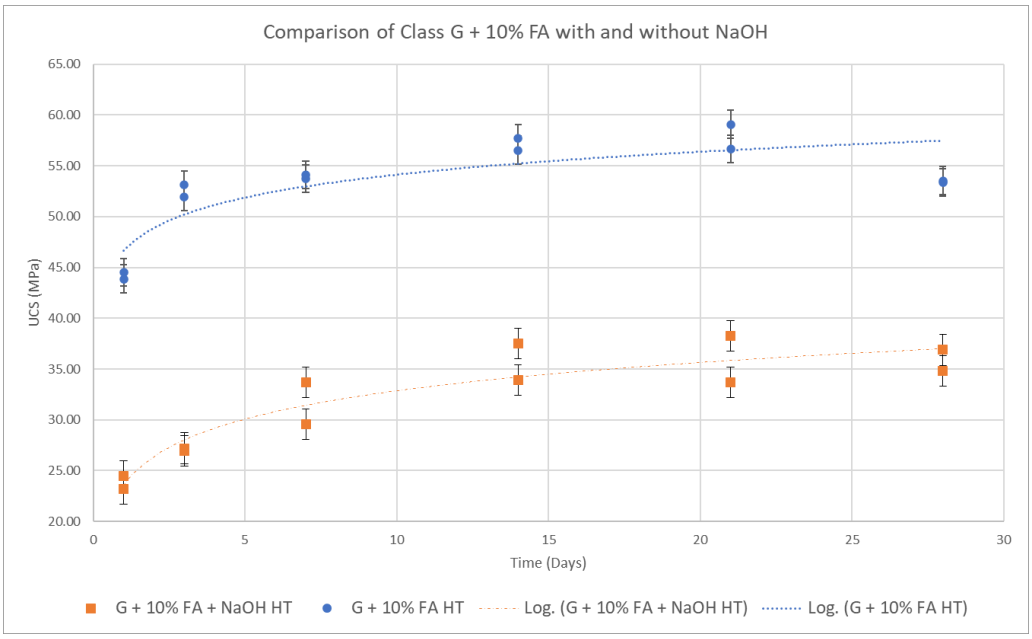

Figure 25. Class G + 10% FA + NaOH high temperature.

4.1.6 Class G + 20% fly ash + NaOH,

The result of adding sodium hydroxide for 20% fly ash, which is half of the weight of the fly ash, there is a slight increase of the compressive strength as seen in **Figure 26**, where on day 1 the samples had about 6 MPa and ended having 10.7 MPa by day 28.

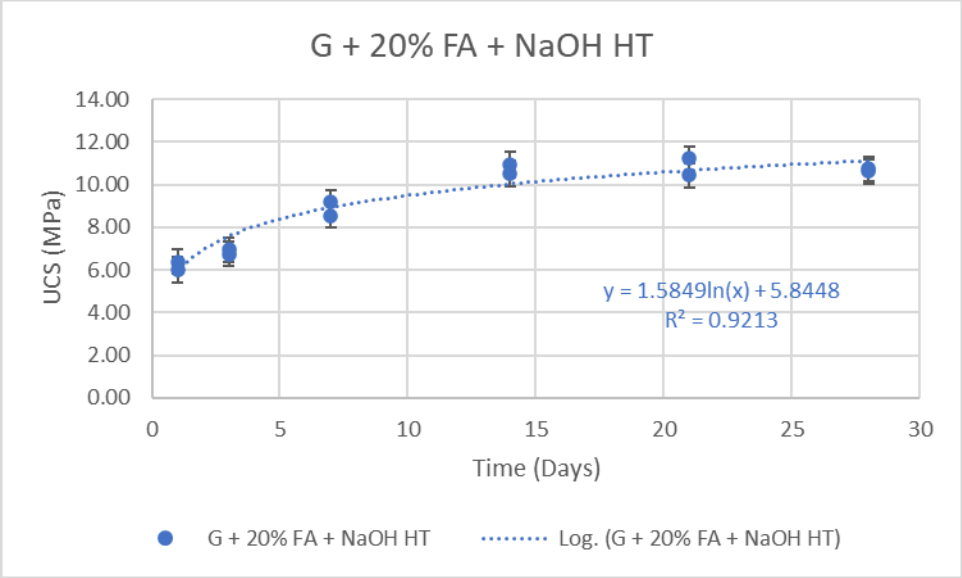

Figure 26. Class G + 20% FA + NaOH high temperature.

In comparison to the original recipe of Class G + 20% FA, the development of the compressive strength has been slowed down. The overall decrease of the compressive strength during the testing of most of the samples is in the order of 6 folds, refer to **Figure 27**.

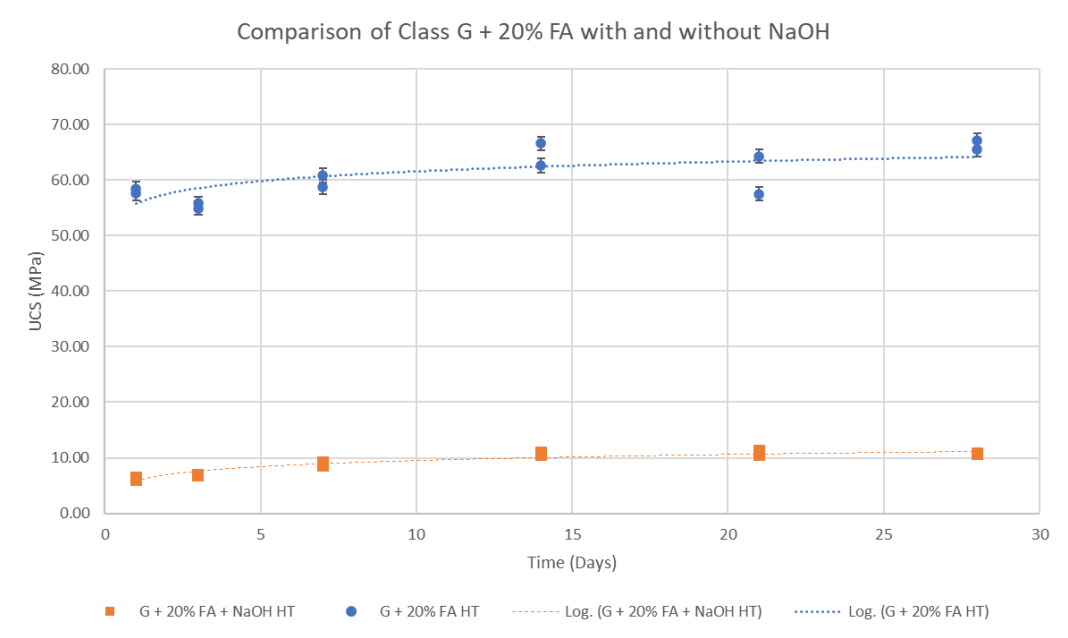

Figure 27. Comparison of class G + 20% FA with and without NaOH.

4.1.7 Class G + 30% fly ash + NaOH.

Once again, the outcome of introducing sodium hydroxide, but this time for the class G + 30% fly ash recipe, the increase of the compressive strength is minimal over the course of the testing as seen in **Figure 28**, starting at 6 MPa on day 1 and finishing with a compressive around 9 MPa on day 28.

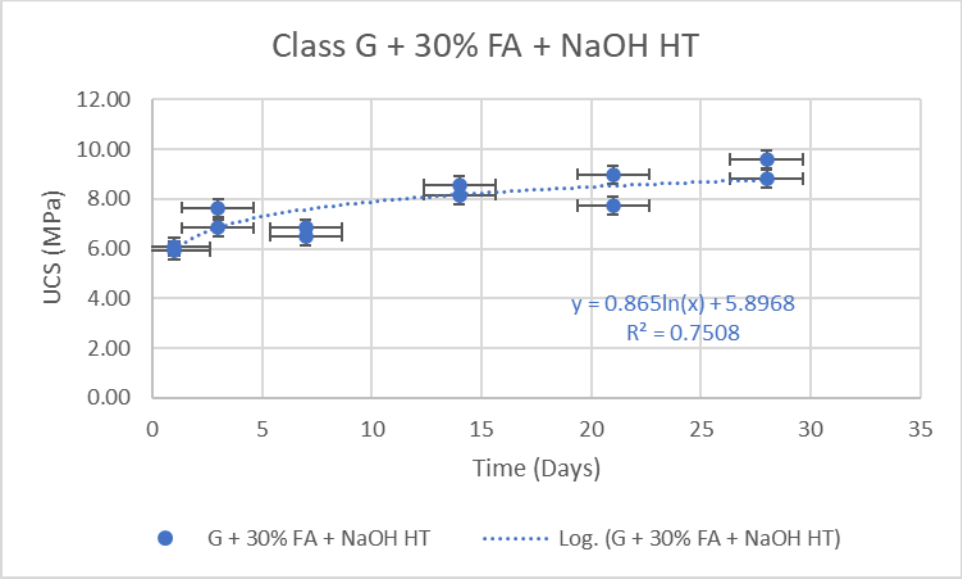

Figure 28. Class G + 30% FA + NaOH high temperature.

When contrasting with the initial Class G + 30% fly ash recipe, once more the development of the compressive strength has been delayed, decreasing it from six to seven times, related to **Figure 29,** during all the duration of the tests that were carried out.

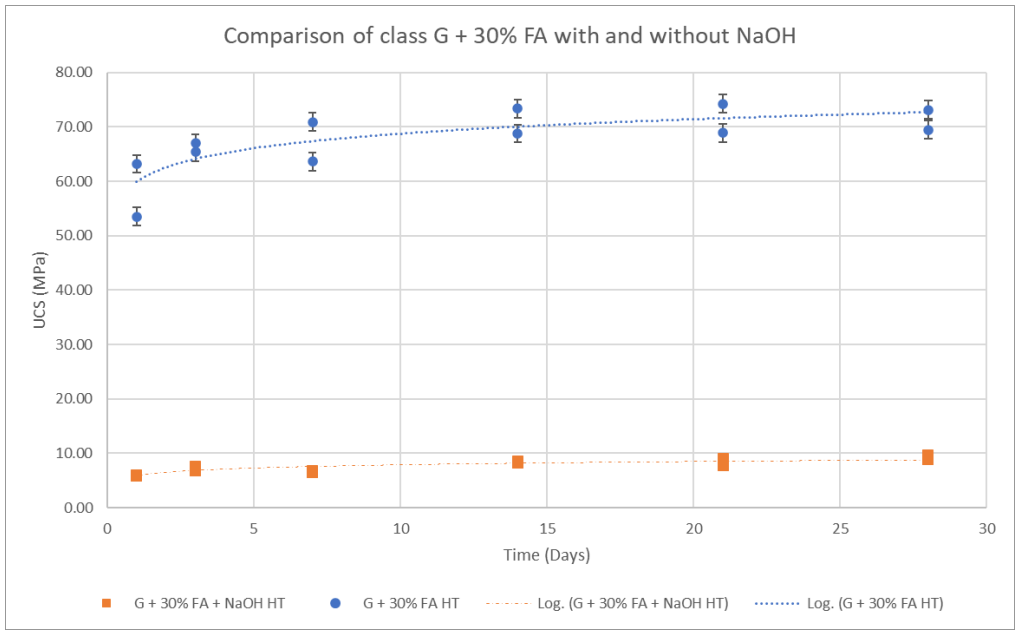

Figure 29. Comparison of class G + 30% FA with and without NaOH.

4.2 Results of Thermal properties measured through the Keithley 2400 meter with TPS-3.

4.2.1 Conductivity.

The control sample, identified as class G cement, was used as the initial reference point for comparison, as shown in the **Figure 30,** the average thermal conductivity had a range between a minimum of 1.138 W/mk and a maximum of 1.55 W/mk, ultimately setting at 1.397 W/mk by day 28.

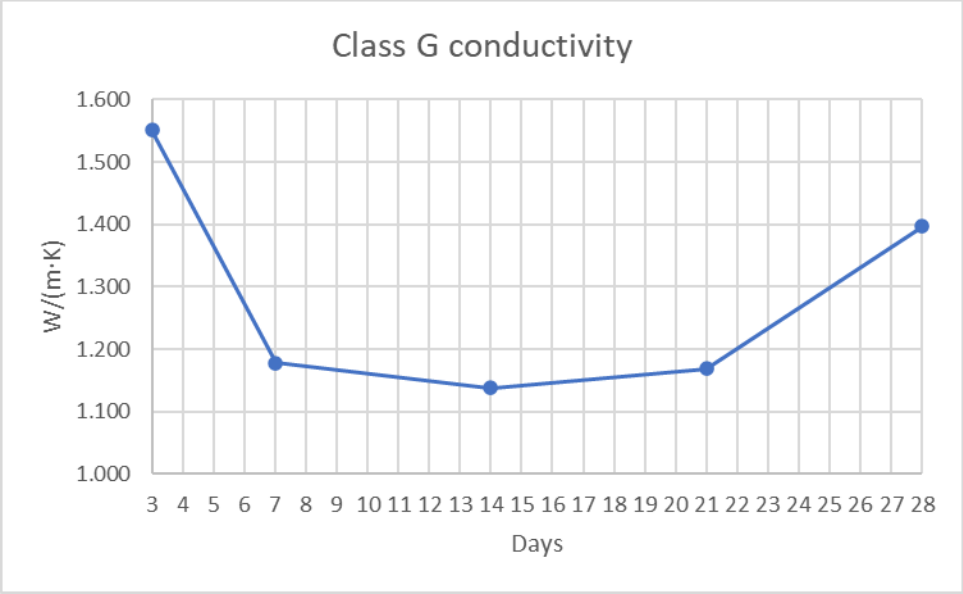

Figure 30. Class G conductivity.

Continuing with the sample of class G + 10% FA, the measured average thermal conductivity exhibited a range of values that fluctuated from 1.081 W/mk to 1.396 W/mk, achieving an average value of 1.12 W/mk by day 28 as depicted in **Figure 31.**

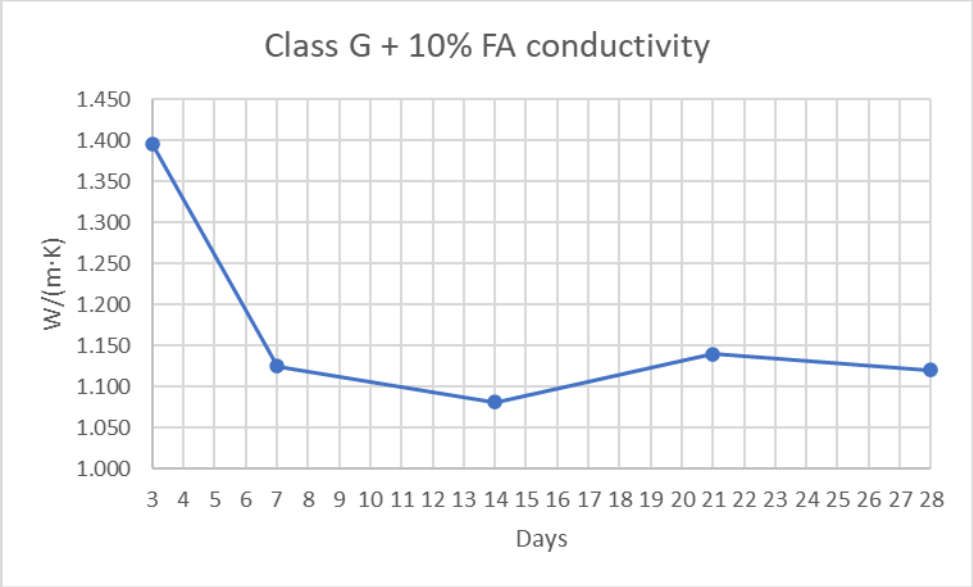

Figure 31. Class G + 10% FA conductivity.

Moving on to the sample of class G + 20% FA, the thermal conductivity of this sample was determined to range from a minimum of 1.065 W/mk to 1.286 W/mk as shown in **Figure 32**, reaching an average of 1.147 W/mk by day 28.

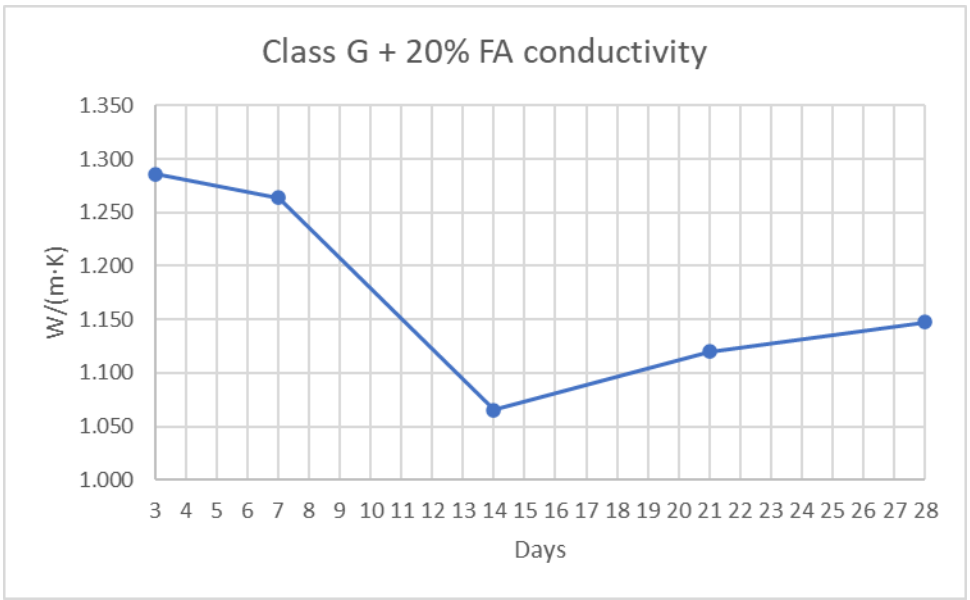

Figure 32. Class G + 20% FA conductivity.

Finally, the thermal conductivity of the sample of class G + 30% FA, was ranging from a minimum of 1.023 W/mk that was reached by day 28 and a maximum value of 1.337 W/mk on day one as can be seen in **Figure 33.**

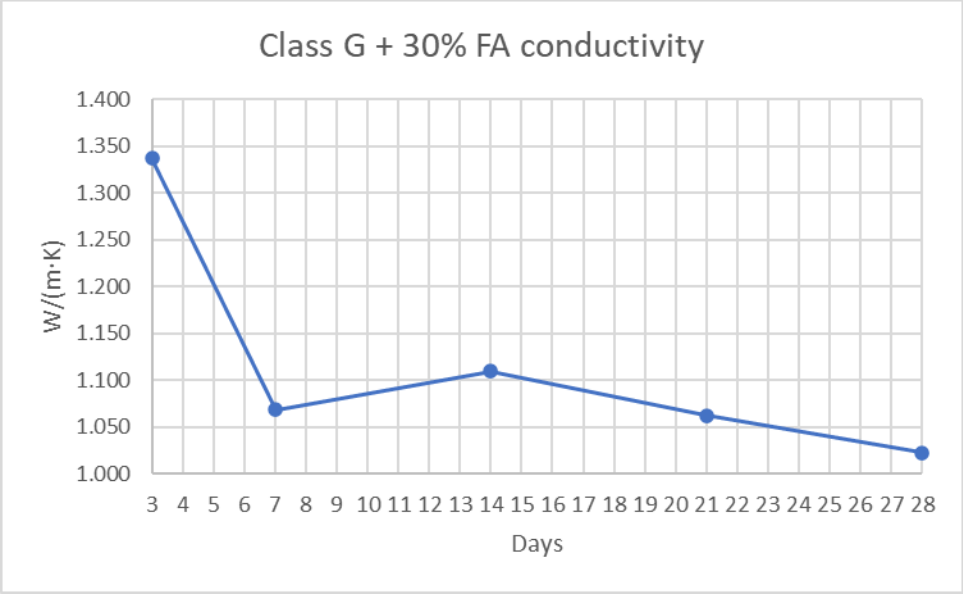

Figure 33. Class G + 30% FA conductivity.

4.2.2 Diffusivity.

Again, the reference values for the comparison point of the thermal diffusivity were measured in the cement Class G samples, where the minimum average value for it was 0.466 mm²/s and its maximum value was 0.805 mm²/s, as depicted in **Figure 34**, which also coincides with the final day of measurement, that is, day 28.

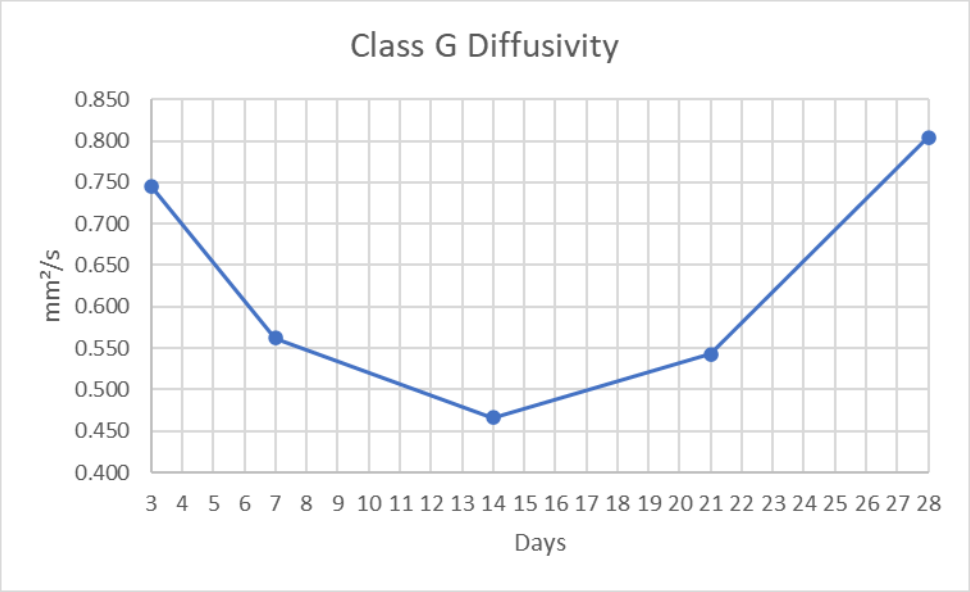

Figure 34. Class G Diffusivity.

Following with the samples made of cement class G + 10% FA it was measured an average thermal diffusivity of 0.389 mm²/s in its minimum point and a maximum thermal diffusivity of 0.661 mm²/s as shown in **Figure 35**, reaching 0.47 mm²/s by day 28.

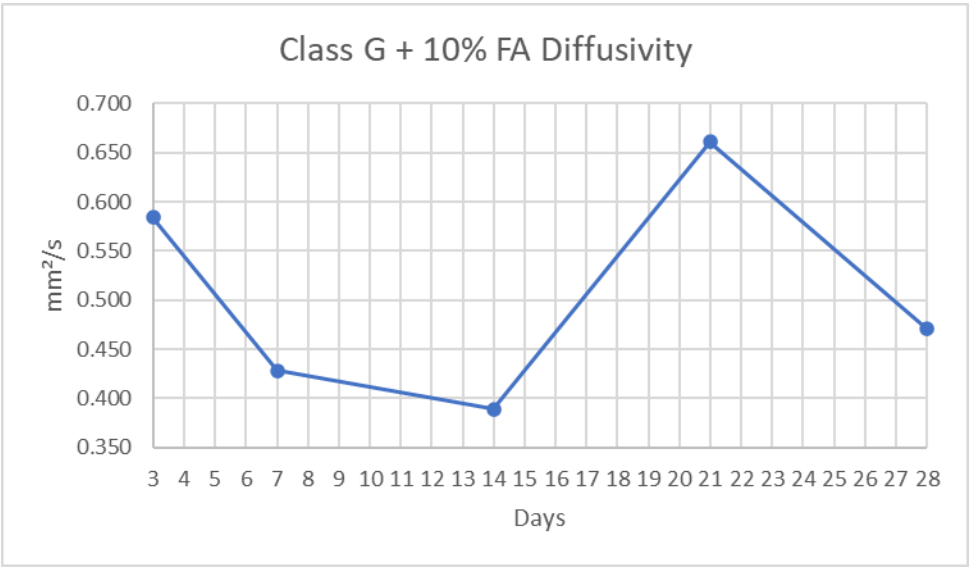

Figure 35. Class G + 10% FA Diffusivity.

Next, when the thermal diffusivity of the cement class G + 20% FA was measured an average minimum of 0.332 mm²/s and maximum of 0.532 mm²/s, eventually setting 0.488 mm²/s on day 28 as displayed in **Figure 36.**

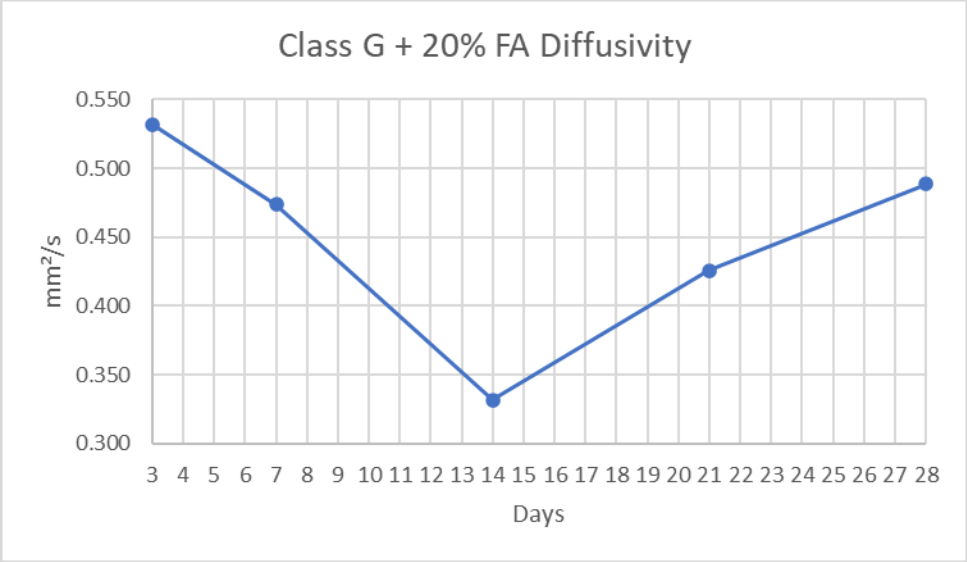

Figure 36. Class G + 20% FA Diffusivity.

Finally, the sample made of class G cement + 30% FA was measured and obtained an average diffusivity value that ranged from a minimum of 0.492 mm²/s which coincides with the last day of measurements to a maximum of 0.581 mm²/s as illustrated in **Figure 37.**

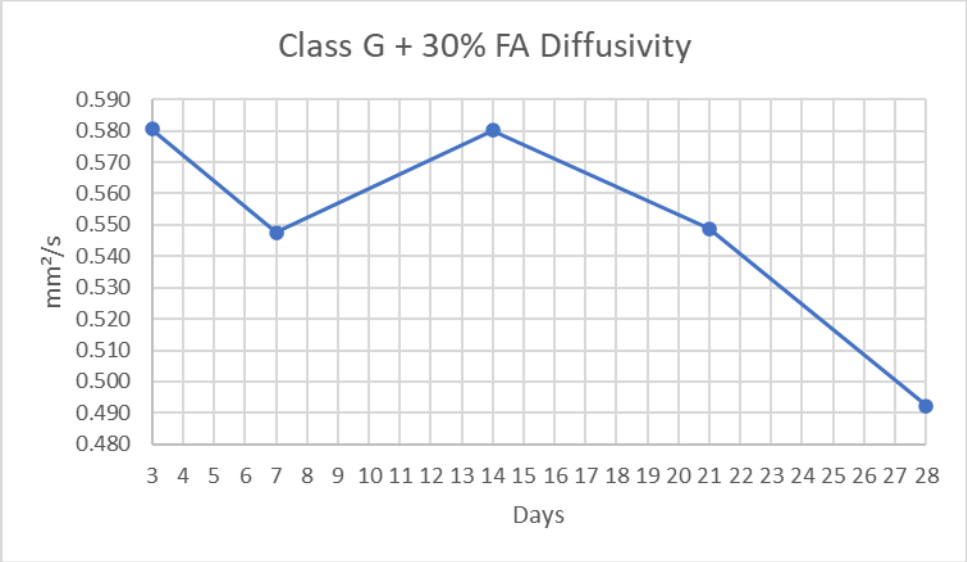

Figure 37. Class G + 30% FA Diffusivity.

4.2.3 Heat capacity.

Once again, a cement class G sample was used as a point of reference for the comparison of heat capacity, the respective values for this sample ranged from a minimum of 1.758 MJ/(m³K) which also correspond to the final day of measurement, being day 28, to a maximum of 2.457 MJ/(m³K) as shown in **Figure 38.**

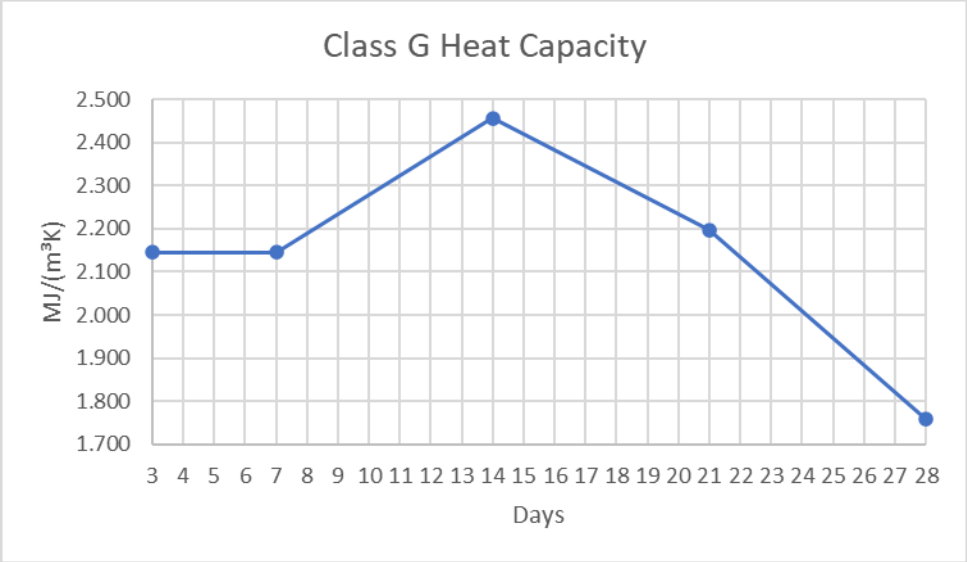

Figure 38. Class G Heat Capacity.

Moving on to the measurements of heat capacity of the cement class G + 10% FA sample, that fluctuated from a minimum of 1.728 MJ/(m³K) to a maximum of 2.803 MJ/(m³K), getting a value of 2.578 MJ/(m³K) by day 28 as observed in **Figure 39.**

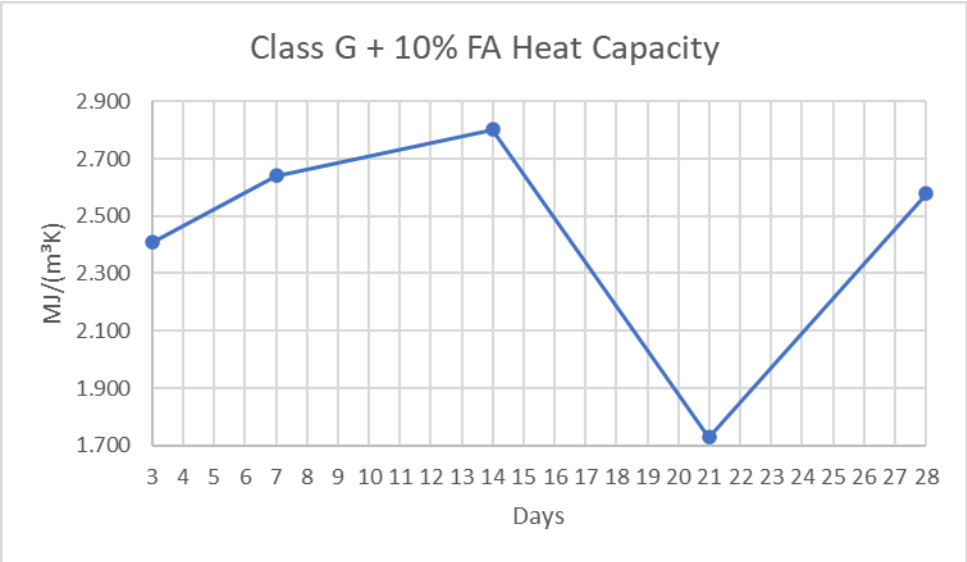

Figure 39. Class G + 10% FA Heat Capacity.

Likewise, the values for the heat capacity were measured on the sample made of class G cement + 20% FA, the values obtained for this specific sample varied from 2.465 MJ/(m³K) which is the minimum value and is the last measurement that was made on day 28, to a maximum value of 3.295 MJ/(m³K), as exposed on **Figure 40.**

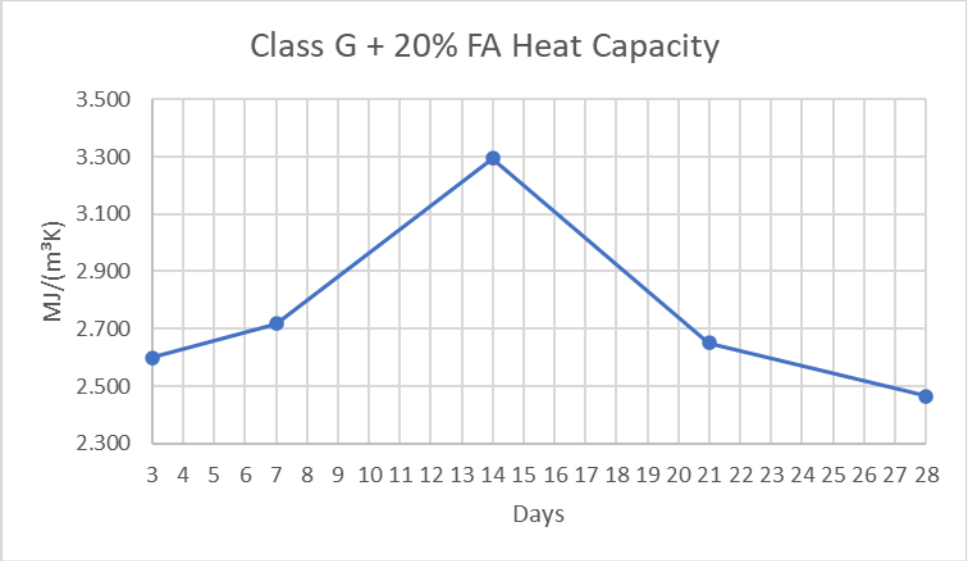

Figure 40. Class G + 20% FA Heat Capacity

Equally, when the heat capacity of the sample made of class g cement with and addition of 30% FA was measured, this property had a range between 1.96 MJ/(m³K) to 2.343 MJ/(m³K), achieving a value of 2.132 MJ/(m³K) by day 28 as depicted in **Figure 41.**

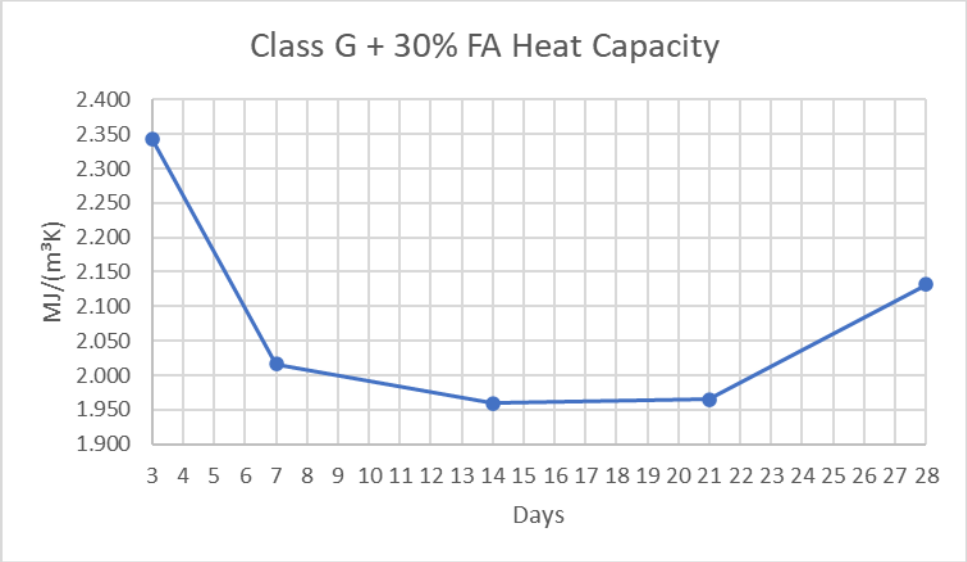

Figure 41. Class G + 30% FA Heat Capacity.

4.2.4 Effusivity.

Once more, a sample from the G class of cement served as the benchmark for assessing the Effusivity, The Effusivity values of this specific sample ranged between a minimum of 1562.797 W√s/(m²K), corresponding to the final day of measurement which is day 28, to a maximum of 1810.138 W√s/(m²K) as illustrated in **Figure 42**.

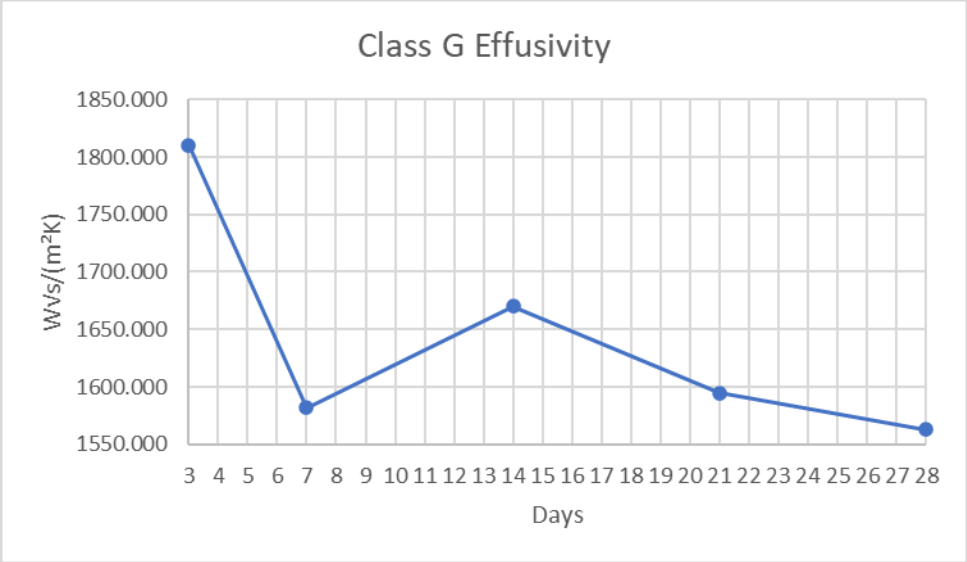

Figure 42. Class G Effusivity

The measurements of the effusivity for the class G + 10% FA fluctuated between a minimum value of 1402.799 W√s/(m²K) to a maximum of 1830.501 W√s/(m²K). by day 28 as depicted in **Figure 43**, the sample recorded a value of 1670.451 W√s/(m²K).

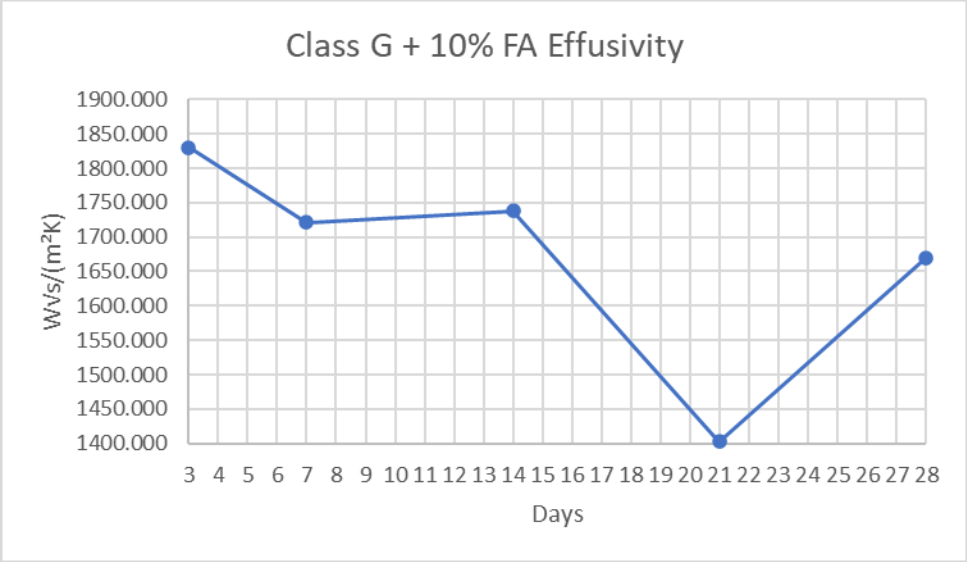

Figure 43. Class G + 10% FA Effusivity.

When the effusivity of the sample made of cement class G + 20% FA the corresponding measurements variated in a range from 1665.384 W√s/(m²K), which is the minimum value and corresponded to day 28 that is the last day of measurement, to a maximum of 1852.965 W√s/(m²K) as shown in **Figure 44**.

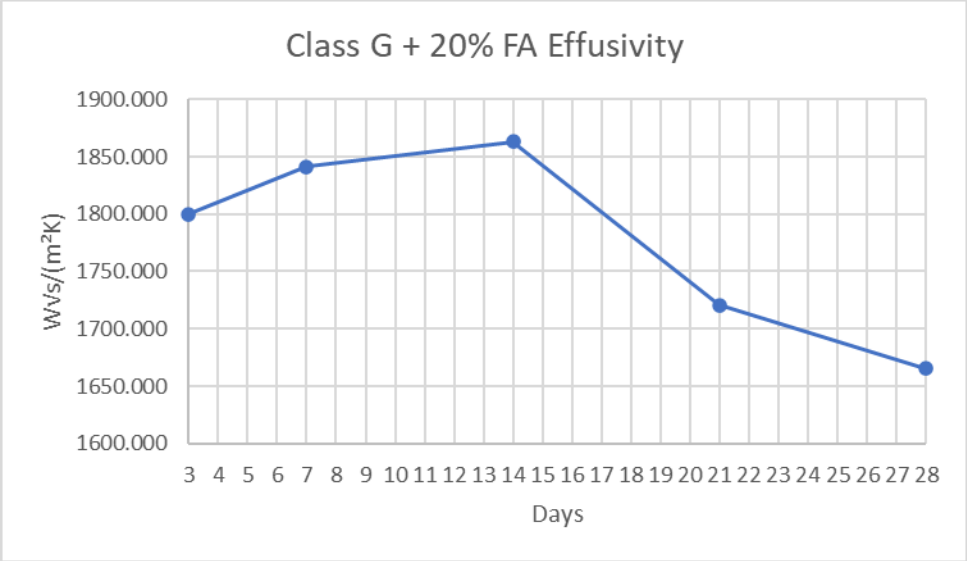

Figure 44. Class G + 20% FA Effusivity.

Finally, the effusivity of the cement class G + 30% FA sample was measured getting a range between 1440.788 W√s/(m²K) and 1762.726 W√s/(m²K), as shown in **Figure 45**, the value of the effusivity of the sample by day 28 was 1468.081 W√s/(m²K).

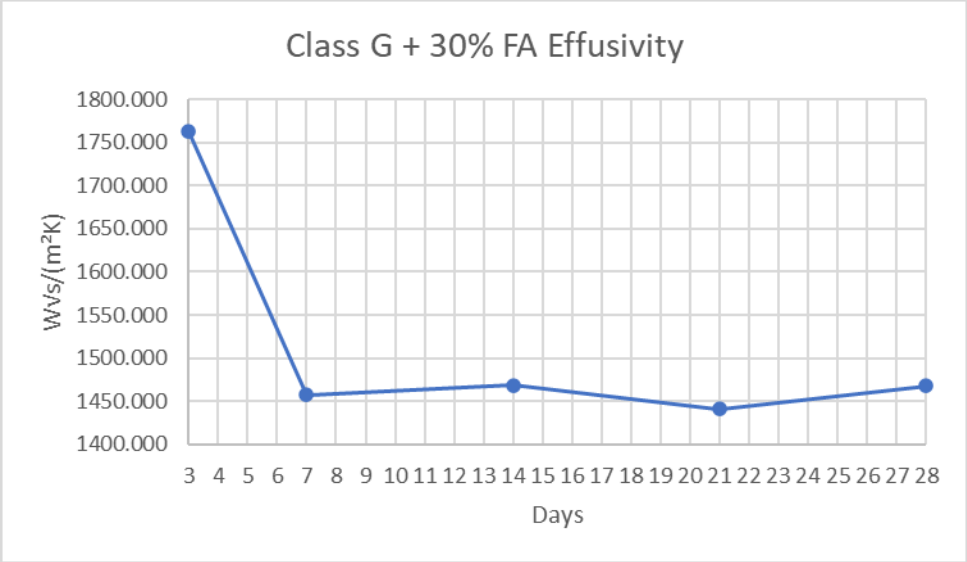

Figure 45. Class G + 30% FA Effusivity.

4.3 Results of Thermal conductivity measured through the Thermtest Portable Measurement Platform.

The initial reference point for comparison was established with the control sample which is class G cement. As seen in **Figure 46** the result of the average thermal conductivity varies between 1.015 W/mk to 1.054 W/mk ending up with 1.033 W/mk on day 28.

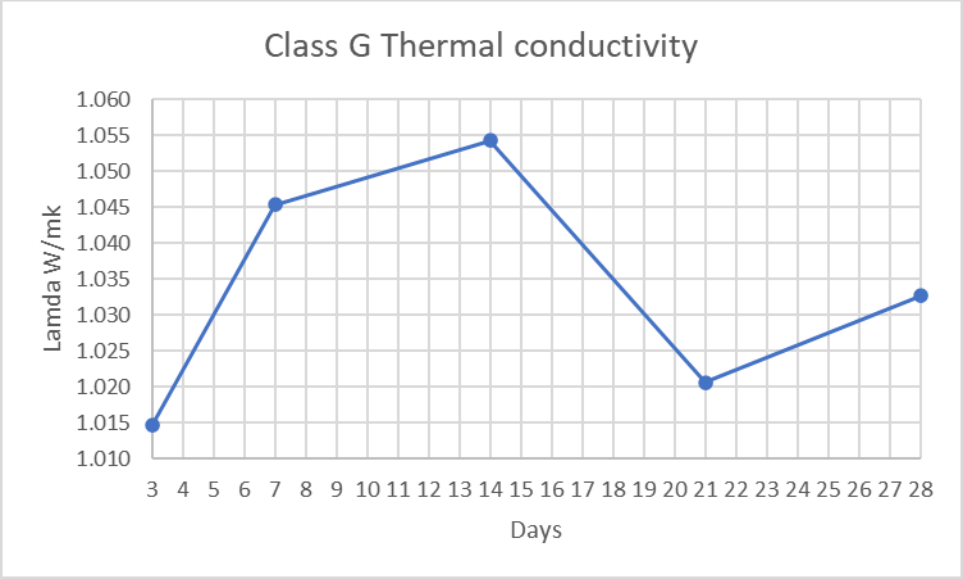

Figure 46. Class G Thermal conductivity.

Moving on to class G + 10% FA samples, the value of the average thermal conductivity of these samples fluctuates from a minimum of 0.939 W/mk to a maximum of 1.044 W/mk, finally getting an average of 1.04 W/mk on day 28 as depicted **Figure 47**.

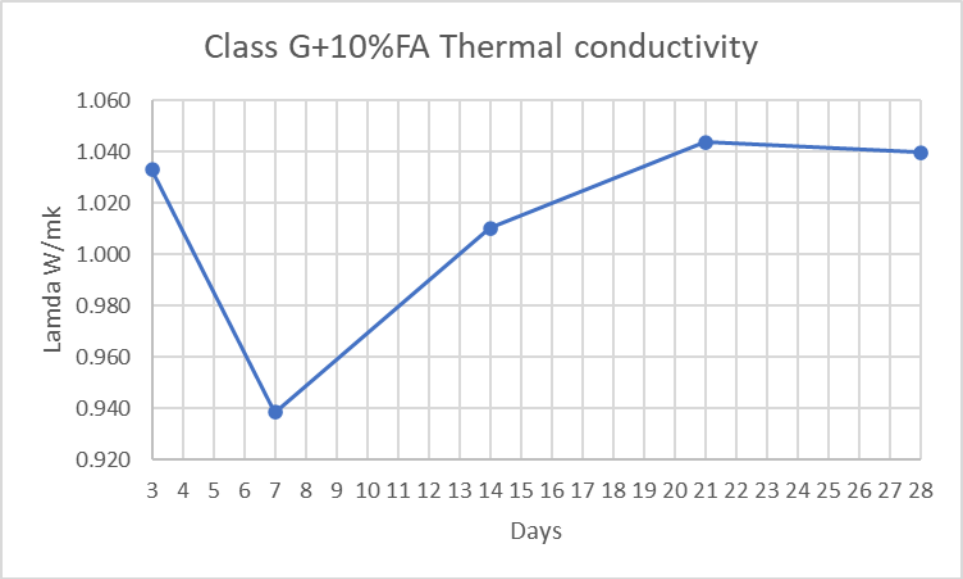

Figure 47. Class G+10%FA Thermal conductivity.

Next, the average value for the thermal conductivity of the class G + 20% FA samples swings from a lower value of 1.114 W/mk to a maximum value of 1.167 W/mk as seen in **Figure 48**, achieving a final value of 1.134 W/mk by day 28.

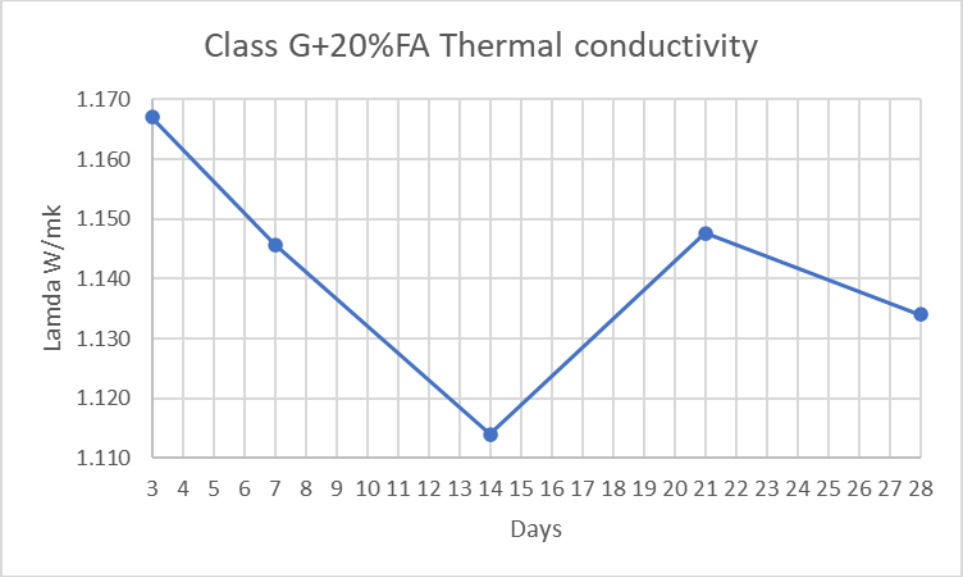

Figure 48. Class G+20%FA Thermal conductivity.

Finally, the thermal conductivity value of the samples of class G + 30% FA **Figure 49**, changes between a minimum average value of thermal conductivity of 1.03 W/mk and a maximum average value of 1.095 W/mk, finishing with a value of 1.087 W/mk on day 28.

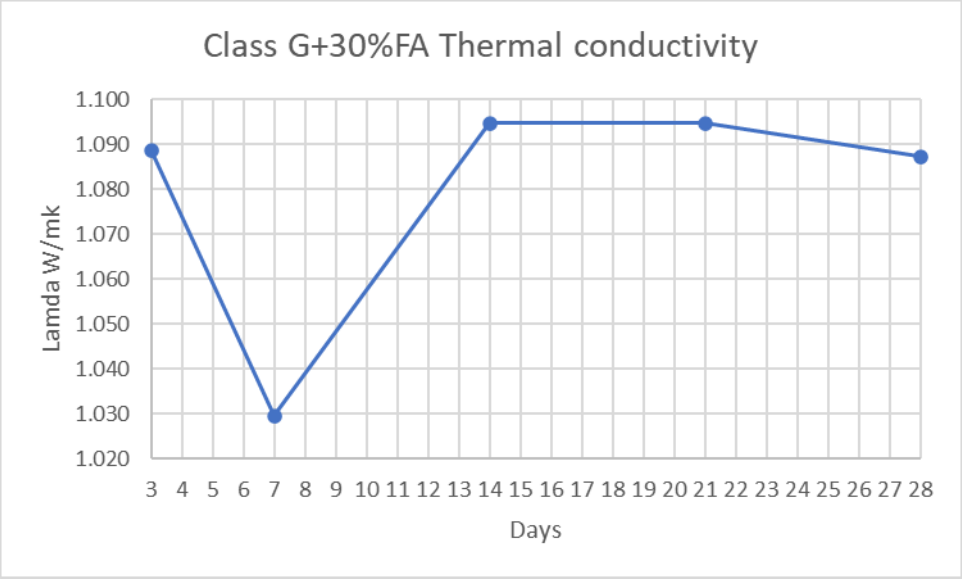

Figure 49. Class G+30%FA Thermal conductivity.

4.4 Density.

Figure 50 , shows the density of the different samples that were used for the thermal properties experiment, where the sample with the lowest density is the control sample that is to say the class G cement sample, followed by the sample with an addition of 10% fly ash that experienced an increment of the density of 2%, continuing with the sample with addition of 30% fly ash that had an increment of 6%, and finishing with the sample with an addition of 20% fly ash with an increase of 7% of the density compared the control samples.

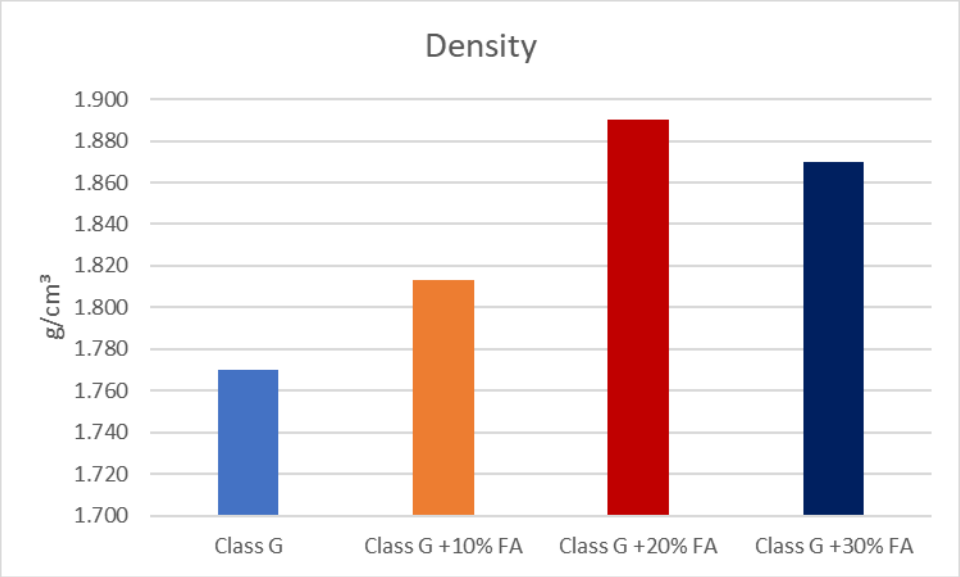

Figure 50. Density of all the samples.

5 Discussion.

This section is going to describe, analyze and interpret the findings from the previous part that are all included. Additional graphs were done in order to be able to understand and make comparisons across the different results for both compressive strength and thermal properties for all the samples used during the research.

5.1 Compressive strength.

A tendency was identified according to the results obtained during the testing of the different samples tested at room temperature. where the addition of fly ash to the mixture improves the overall performance of the samples enhancing the development of the compressive strength in all the scenarios evaluated. Likewise, the addition of a greater percentage of fly ash the greater the increase of the compressive strength of the samples, being the sample with 30% fly ash the strongest of all of them as seen on **Figure 51.**

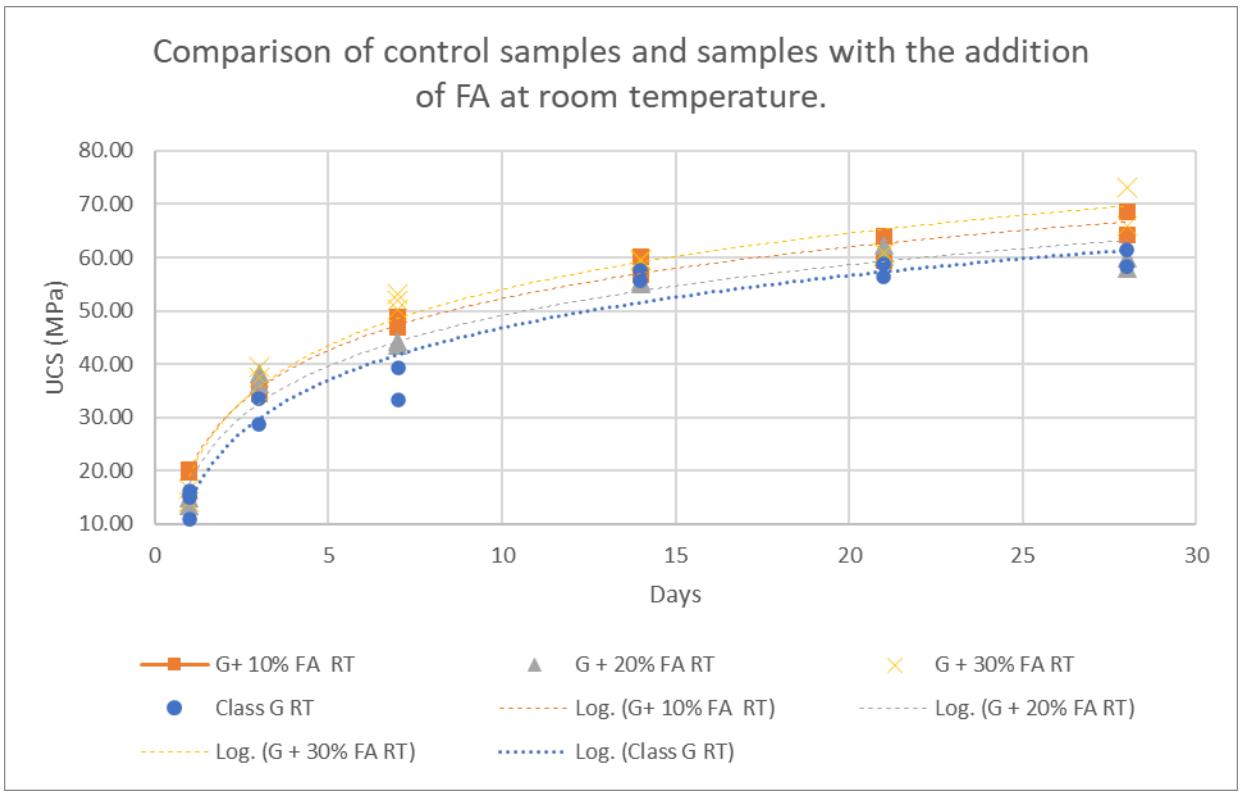

Figure 51. Comparison of control samples and samples with the addition of FA at room temperature.

Similarly, the introduction of fly ash in the mixture had a beneficial effect on the samples' overall performance, increasing the development of compressive strength across all the evaluated instances, according to a tendency seen in samples exposed to high. Also, as in the different scenarios at room temperature, the larger the amount of fly ash in the mixture the better the development of the compressive strength, as shown in **Figure 52**, the samples that had 30% fly ash has the greatest compressive strength among all the other samples.

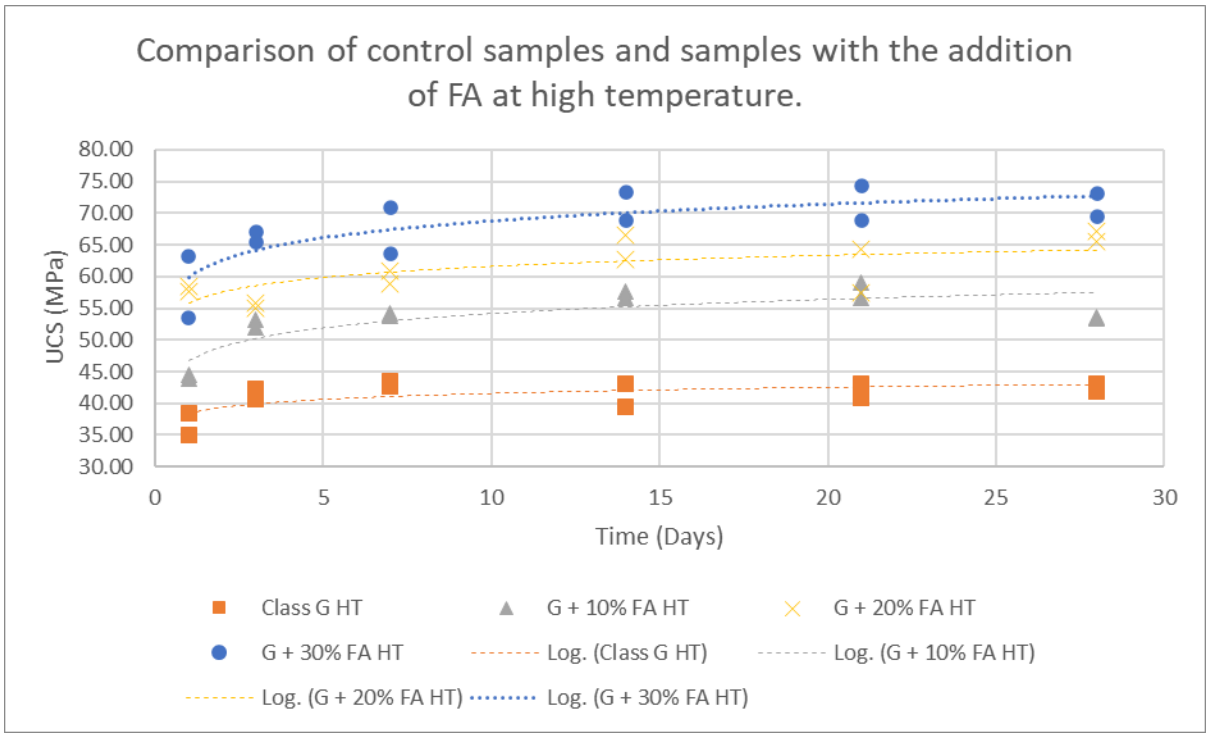

Figure 52. Comparison of control samples and samples with the addition of FA at high temperature.

This behavior can be explained because of the incorporation of the added strength-providing product, in this specific study is the fly ash, increasing the original value of the compressive strength, meaning the pozzolanic activity of this additive prevails, promoting the enhancement of this mechanical property due the facilitation of formation of additional strength-contributing products, specifically C-S-H and C-A-S-H (Akmalaiuly et al., 2023).

On the other hand, when sodium hydroxide is added to the mixture, being half of the weight of the fly ash, the behavior of the samples is shifted **Figure 53**. Where the samples with the most fly ash, hence, the samples with the most sodium hydroxide are the ones with the worst development of compressive strength.

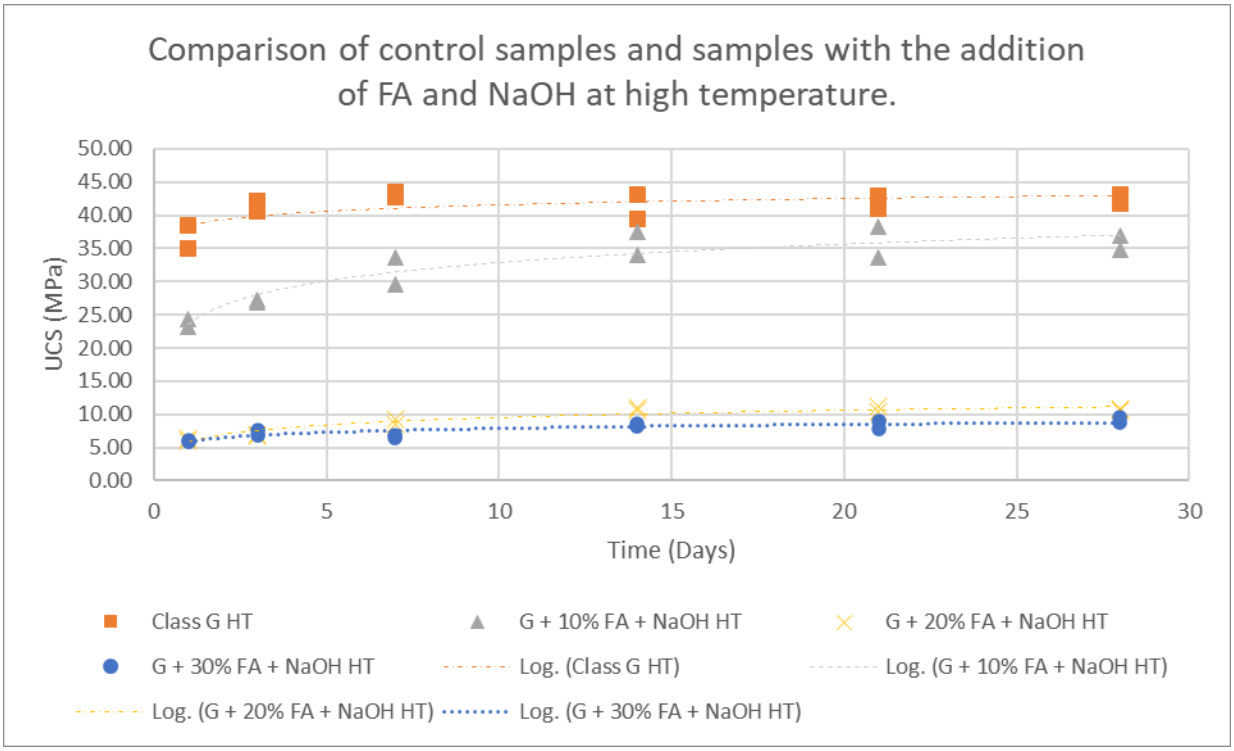

Figure 53. Comparison of control samples and samples with the addition of FA and NaOH at high temperature.

This shift in the behavior is explained by the increase of the pH values due the addition of sodium hydroxide into the mixture, which prevents the formation of aluminum hydroxide, leading to a much higher dissolved aluminum concentration, likewise because of the higher presence of alkali hydroxide the uptake of aluminum in C-S-H decreases, being stronger at higher pH values, thus leading to a poor development of the compressive strength(Barzgar et al., 2020).

5.2 Thermal properties measured through the Keithley 2400 meter with TPS-3.

During the experiment, the conductivity of all the different samples was measured using the Keithley 2400 meter with TPS-3. However, the behavior of these samples when the conductivity was measure was fluctuating significantly over the duration of the test, as depicted in **Figure 54**, suggesting that the conductivity has not reached stability during the testing period.

Due to the fluctuations in the values of the conductivity, it was challenging if not impossible to determine and analyze the real effect of different percentages of fly ash as an additive in class G cement. Thus, making it difficult to establish a clear relationship between the percentage of fly ash added and the value obtained for thermal conductivity in the cement sample. Additionally, the thermal conductivity of the control sample itself, class G cement, also displayed uncertainty, showing that even without the addition of fly ash there were variations in the conductivity. Making it challenging to precisely assess the effects of fly ash as an additive for thermal conductivity purposes.

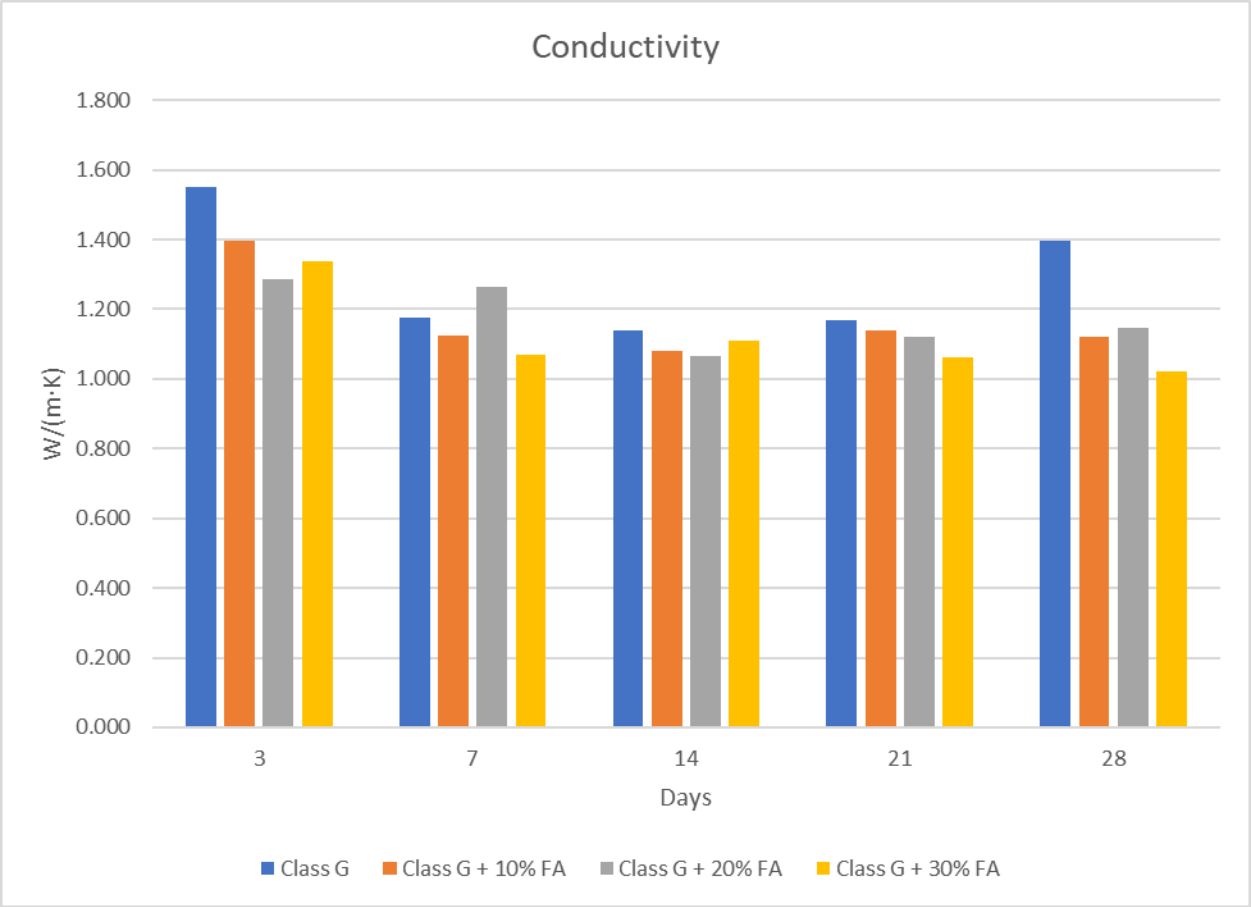

Figure 54. Conductivity (Keithley 2400 meter with TPS-3).

Moving on to the diffusivity of the samples, a similar behavior as the one in thermal conductivity was measured, there were significant fluctuations in the diffusivity values of all the samples throughout the period of testing, as seen in **Figure 55**. Implying that the diffusivity has not achieved stability by the end of the measurements. Therefore, it was challenging to identify a clear and stable trend in how the diffusivity values behave throughout time, making difficult the forecasting of the future values of the different samples that were under testing. Likewise, the fluctuation of the diffusivity has impeded the establishment of a correlation between the variation of the percentage of fly ash added to class G cement and their effect on the measured property.

Again, there is a major fluctuation in the control sample, hiding the possible effects that different percentages of fly ash added to the class G cement may have over the thermal diffusivity. Consequently, it makes it impossible to get any meaningful conclusion of what the real effects of this additive are.

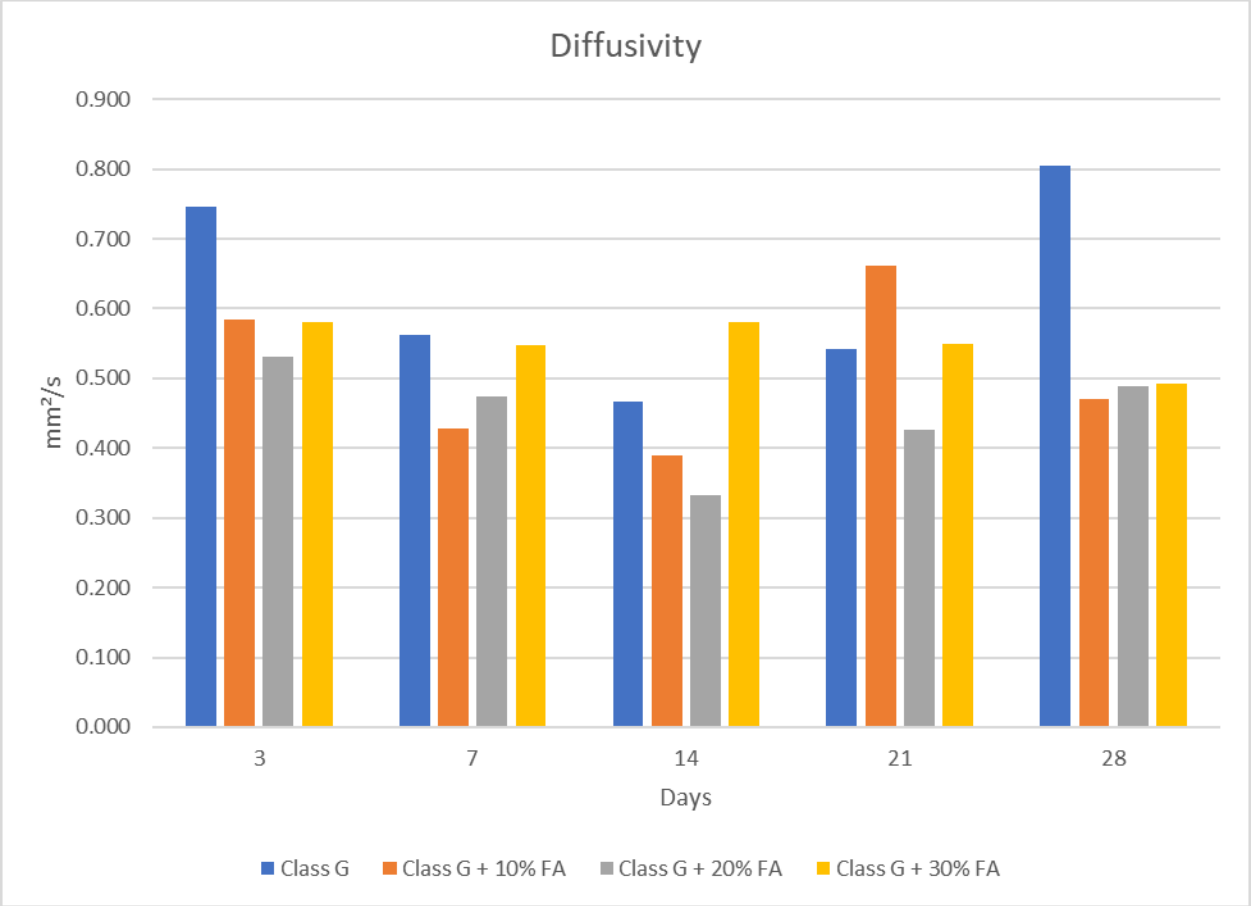

Figure 55. Diffusivity (Keithley 2400 meter with TPS-3).

A similar behavior was measured for the heat capacity of the different samples, where the fluctuation of the heat capacity was not as significant as the ones measured for thermal conductivity and thermal diffusivity. While the fluctuations were less pronounced as depicted in **Figure 56**, they are still existing and were noticeable during the duration of the testing. As a result of those fluctuations, drawing conclusions about the effects that varying the percentage of fly ash in class G cement has over the heat capacity end up being particularly challenging, hence, stablishing a consistent and reliable trend will not be possible. On the other hand, the measurements of heat capacity faced difficulty in identifying the real behavior of the neat class G cement, in other words class G cement without additives in this specific scenario without fly ash.

These values obtained for the neat sample cannot be compared with confidence with the ones that had different percentages of fly ash, therefore, no conclusion can be drawn.

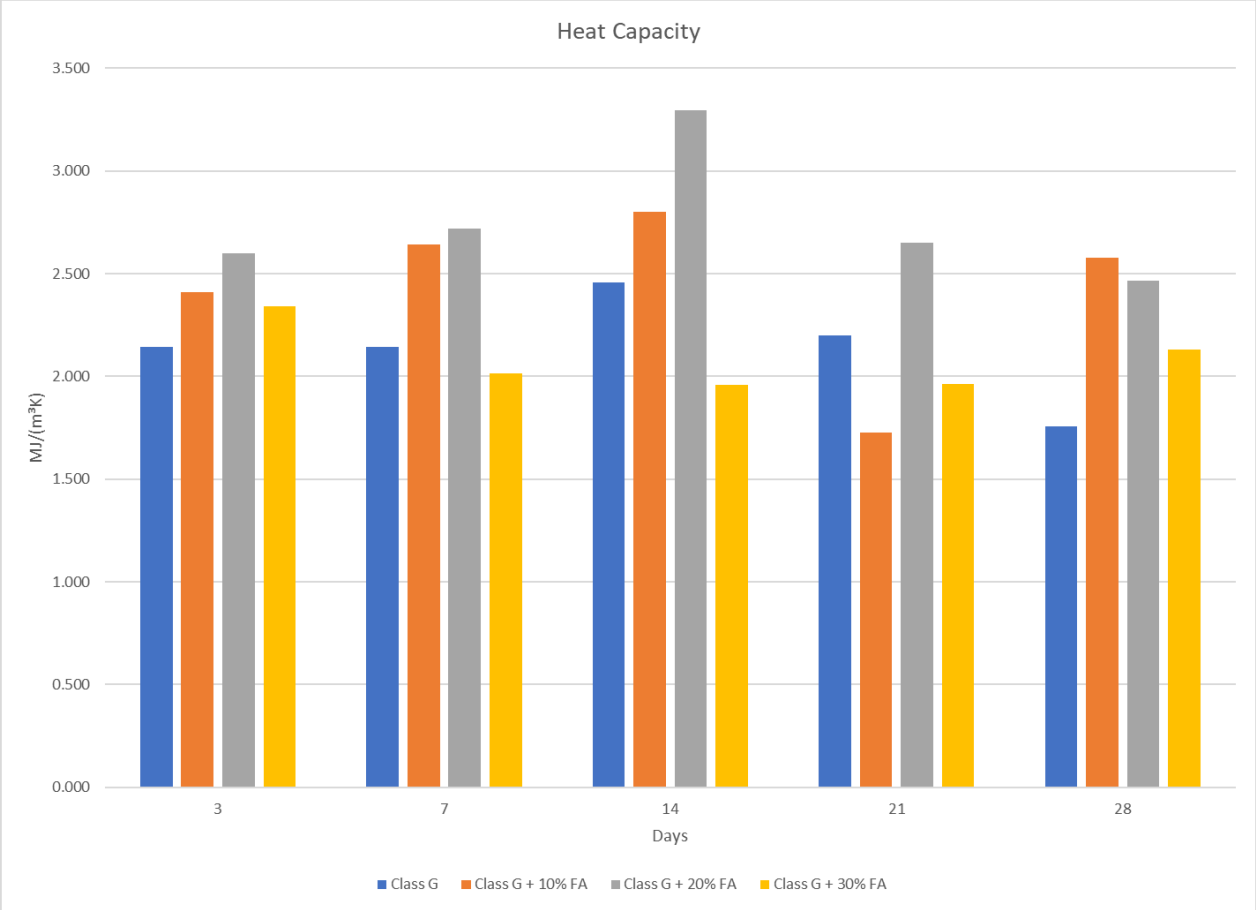

Figure 56. Heat capacity (Keithley 2400 meter with TPS-3).

Finally, the effusivity of the samples was measured and like the previous measurements for the other three thermal properties, the respective measurements of the effusivity displayed consistent variations over time. This fluctuation in effusivity measurements made it challenging to determine and analyze the effects of incorporating different percentages of fly ash into class g cement, which has prevented a clear understanding of how the variation of percentages has influenced the effusivity of the samples as displayed in **Figure 57**. Similarly, difficulty was encountered in identifying the inherent behavior of class G cement (without additives) concerning

effusivity. Without a stable baseline representing the performance of the effusivity of class g cement, the comparison of the results of varying fly ash percentages with the ones obtained from the control sample was not possible.

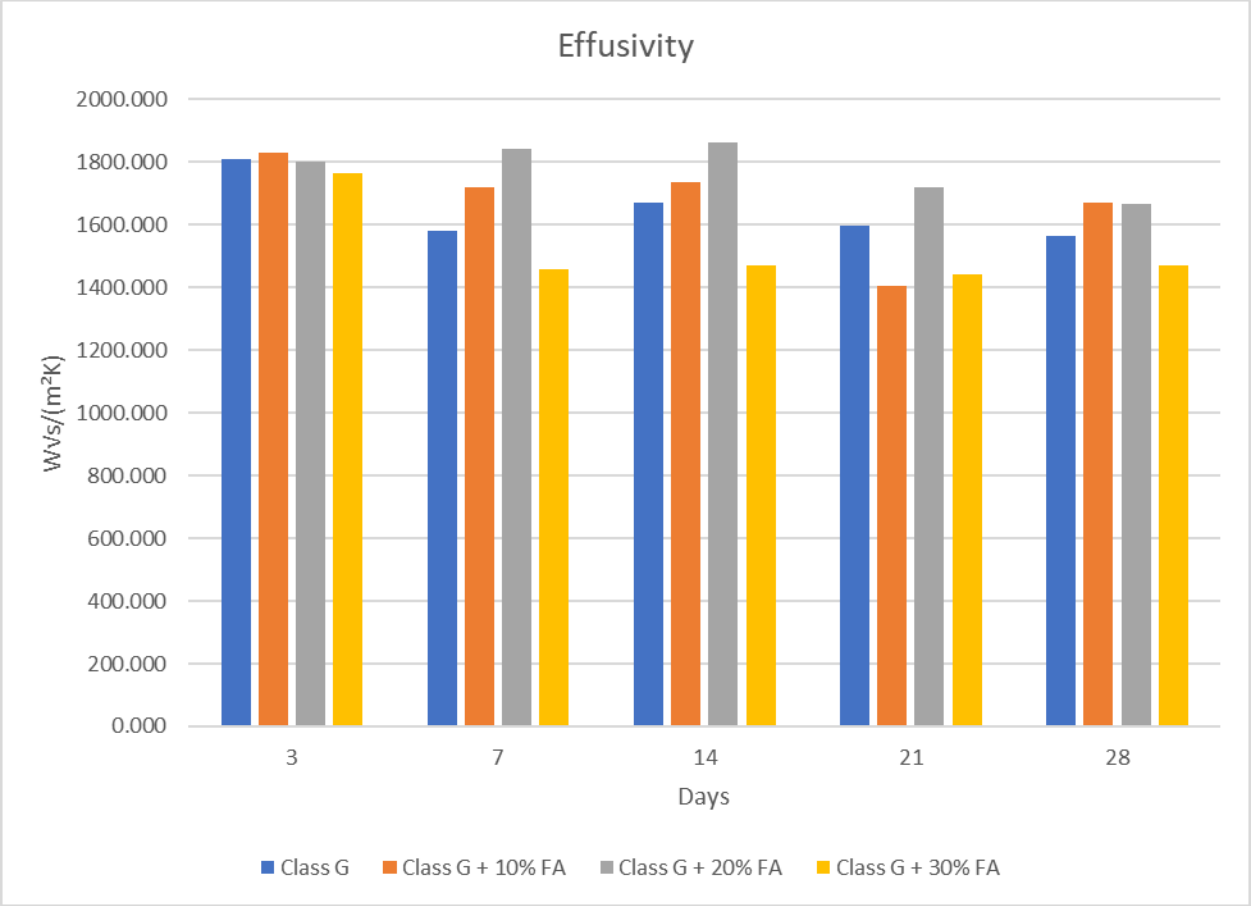

Figure 57. Effusivity (Keithley 2400 meter with TPS-3).

5.3 Thermal conductivity measured through the Thermtest Portable Measurement Platform.

During the experiment, the conductivity of all the different samples of cement were measured using the Thermtest Portable Measurement Platform. In contrast to the previous measurements done using the Keithley 2400 meter with TPS-3, the conductivity measurements showed mild fluctuations as displayed in **Figure 58**. Despite of those mild fluctuations, the

measurements of the conductivity values remined stable enough to observe a tendency throughout the duration of the test, allowing the identification of a point of comparison using the values of the class G cement sample, helping in understanding how the conductivity changes as the percentage of fly ash varies. Overall, the addition of fly ash to the class g cement has increased the thermal conductivity of all the samples that were tested, seeing the highest increment, about 9.8%, when 20% fly ash was added to the mixture, and the least increment, around 0.68%, when 10% fly ash was added to the mixture, these results corresponding to the end of the experiment (Day 28).

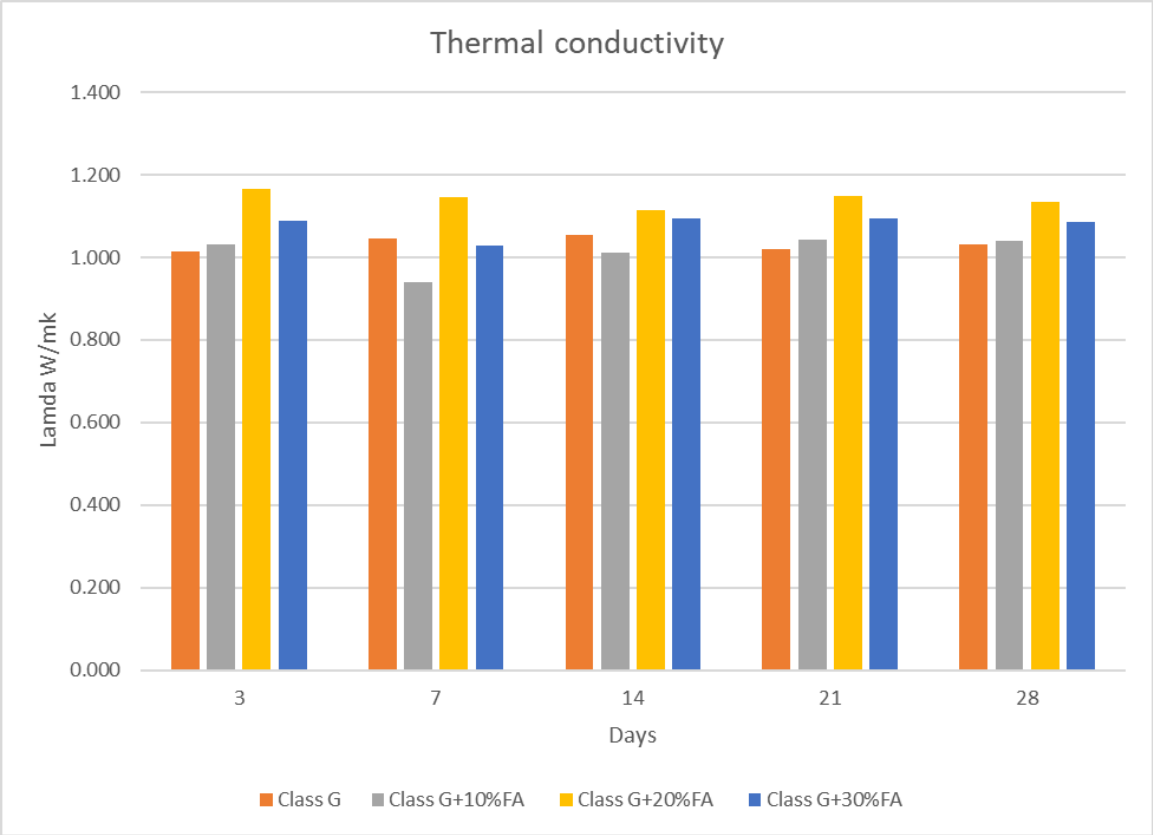

Figure 58. Conductivity (Thermtest Portable Measurement Platform).

These findings were congruent with the values obtained when compared to the density of the samples as seen in **Figure 50**. Therefore, it can be said that the density may have an influence on the thermal conductivity of the samples. The higher the density of the sample, the higher the

thermal conductivity would be. Similar conclusions and findings were reached by (Misri et al., 2018) and (Shafigh et al., 2020). However, these preliminary results are not totally reliable since it has been demonstrated in a previous study (Abid, Romero Tellez, et al., 2023) where different samples were measured for a period of 305 days, where the results obtained still showed minor fluctuation though the duration of the experiment, nevertheless, it is possible to see that the thermal conductivity is reaching a stable value and the trend of the sample is easily identified as seen in **Figure 59.**

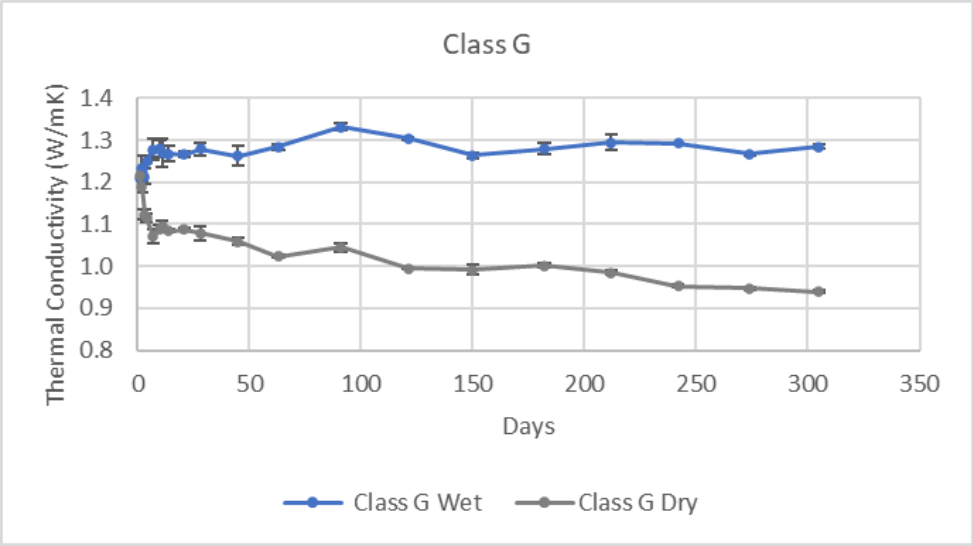

Figure 59. Thermal conductivity values of class G cement after 305 days of curing (Abid et al, 2023)

6 Conclusions

This research shows a dedicated and structured investigation of cement compressive strength measurements of neat class G cement, and class G cement with the addition of fly ash in different percentages by weight of cement with and without sodium hydroxide. Additionally, comprehensive research focused on the measurement of the thermal properties of class G cement with and without the addition of fly ash with two different types of equipment.

- An analytical examination has established a direct correlation between the increase of the percentage of fly ash by weight of class G cement and a consequential enhancement in compressive strength. Always achieving a higher value for this property than neat class G cement.
- The increase of the compressive strength remains consistent and keeps the trend across varying environmental conditions, in other words, encompasses both room and high temperatures.
- Fly ash has the potential to significantly improve the mechanical properties of cement composites, as evidenced by the increase of the compressive strength with a higher concentration of fly ash, showcasing its effectiveness in different applications, including scenarios characterized by high pressures and high temperatures.
- At elevated temperatures, a recognizable pattern appears, where higher percentages proportions of fly ash led to a consistent increase in compressive strength, on the other hand, under room temperature conditions, the influence of fly ash on compressive strength has a modest effect.

- It has been established a direct correlation between the quantity of sodium hydroxide used in the mixture and the resulting deterioration observed in the samples. This occurrence significantly affects the development of the compressive strength within the samples that were tested.
- The decrease of the compressive strength is explained by the increase in pH values brought on by the addition of sodium hydroxide to the mixture, preventing the formation of aluminum hydroxide and resulting in a significantly higher concentration of dissolved aluminum. Additionally, because of the higher presence of alkali hydroxide, the uptake of aluminum in C-S-H decreases, leading to poor development of compressive strength.
- The thermal properties, which encompass conductivity, diffusivity, heat capacity, and effusivity, were measured utilizing the properties measured through the Keithley 2400 meter with TPS-3. However, it was noted that these properties showed a lack of stability during the respective testing in the neat class G sample, by thereby impeding the establishment of a reliable baseline for the following experiments.
- Likewise, these thermal properties were variating for all the samples that were measured in this study with the Keithley 2400 meter with TPS-3, hence making it impossible to establish a relation between the variation of the percentage of fly ash by weight of class g cement and the change of the thermal properties.
- When the thermal conductivity was measured through the Thermtest Portable Measurement Platform, it was possible to see more consistent measurements in the control sample, class G cement, allowing to establish a baseline which to make comparisons with for the subsequent experiments.

- Similarly, the thermal conductivity of the samples with the different percentages of fly ash showed a more stable behavior measured through the Thermtest Portable Measurement Platform compared to the ones measured with the other equipment, hence making it possible to establish a relation between the addition of fly ash to the class G cement and the change of the thermal conductivity.

- It has been concluded that the more fly ash incorporated into the class G cement sample the more is going to be the increment of the thermal conductivity. This being true up to 20% fly ash added by weight of cement. When 30% fly ash by weight of cement was added it was possible to see a slight decrease of the thermal conductivity.

- It was concluded that there might be a direct relation between the density of the samples and the value of the thermal conductivity. Specifically, an increase in the sample density correlates with an increase in the thermal conductivity, in other words, the higher the density of the sample, the higher the thermal conductivity will be.

Bibliography

Abid, K. (2018). *Designing a New Cement Composition Using Agricultural Wastes for Underground Gas Storage*.

Abid, K., Romero Tellez, M. L., & Teodoriu, C. (2023). Experimental Studies on Thermal Properties of Different Class G Cement Composites for Geothermal Well Applications. *Proceedings - SPE Annual Technical Conference and Exhibition*, *2023-October*. https://doi.org/10.2118/214873-MS

Abid, K., Srivastava, S., Tellez, M. L. R., Amani, M., & Teodoriu, C. (2023). Experimental and machine learning study of thermal conductivity of cement composites for geothermal wells. *Geothermics*, *110*. https://doi.org/10.1016/j.geothermics.2023.102659

Aïtcin, P. C. (2016). Portland cement. In *Science and Technology of Concrete Admixtures* (pp. 27–51). Elsevier Inc. https://doi.org/10.1016/B978-0-08-100693-1.00003-5

Akmalaiuly, K., Berdikul, N., Pundienė, I., & Pranckevičienė, J. (2023). The Effect of Mechanical Activation of Fly Ash on Cement-Based Materials Hydration and Hardened State Properties. *Materials*, *16*(8). https://doi.org/10.3390/ma16082959

American Petroleum Institute. (2010). *Specification for Cements and Materials for Well Cementing ANSI/API SPECIFICATION 10A TWENTY-FOURTH EDITION (Identical), Petroleum and natural gas industries-Cements and materials for well cementing-Part 1: Specification*.

American Petroleum Institute. (2016). *Annular Casing Pressure Management for Onshore Wells*.

Bahafid, S., Ghabezloo, S., Faure, P., Duc, M., & Sulem, J. (2018). Effect of the hydration temperature on the pore structure of cement paste: Experimental investigation and micromechanical modelling. *Cement and Concrete Research*, *111*, 1–14. https://doi.org/10.1016/j.cemconres.2018.06.014

Barzgar, S., Lothenbach, B., Tarik, M., Di Giacomo, A., & Ludwig, C. (2020). The effect of sodium hydroxide on Al uptake by calcium silicate hydrates (C[sbnd]S[sbnd]H). *Journal of Colloid and Interface Science*, *572*, 246–256. https://doi.org/10.1016/j.jcis.2020.03.057

Batista da Silva, Í., Martinelli, A. E., Medeiros de Souza, W. R., Cezar de Oliveira Freitas, J., & Felipe Rodrigues, M. A. (2018). Dilatometric behavior and crystallographic characterization of Portland-polyurethane composites for oilwell high-temperature cementing applications. *Journal of Petroleum Science and Engineering*, *169*, 553–559. https://doi.org/10.1016/j.petrol.2018.06.014

Bois, A.-P., Garnier, ; A, & Rodot, F. (2011). *How To Prevent Loss of Zonal Isolation Through a Comprehensive Analysis of Microannulus Formation*. http://onepetro.org/DC/article-pdf/26/01/13/2092545/spe-124719-pa.pdf/1

bp. (2022). *bp Energy Outlook 2022*.

Broni-Bediako, E. (2016). Oil Well Cement Additives: A Review of the Common Types. *Oil & Gas Research*, *02*(02). https://doi.org/10.4172/2472-0518.1000112

Buck, W., & Rudtsch, S. (2011). Thermal Properties. In *Springer Handbook of Metrology and Testing*.

Cahill, A. G., Beckie, R., Ladd, B., Sandl, E., Goetz, M., Chao, J., Soares, J., Manning, C., Chopra, C., Finke, N., Hawthorne, I., Black, A., Ulrich Mayer, K., Crowe, S., Cary, T., Lauer, R., Mayer, B., Allen, A., Kirste, D., & Welch, L. (2019). Advancing knowledge of gas migration and fugitive gas from energy wells in northeast British Columbia, Canada. *Greenhouse Gases: Science and Technology*, *9*(2), 134–151. https://doi.org/10.1002/ghg.1856

Cottrill, A. L., Liu, A. T., Kunai, Y., Koman, V. B., Kaplan, A., Mahajan, S. G., Liu, P., Toland, A. R., & Strano, M. S. (2018). Ultra-high thermal effusivity materials for resonant ambient thermal energy harvesting. *Nature Communications*, *9*(1). https://doi.org/10.1038/s41467-018-03029-x

EIA. (2022). *The Distribution of U.S. Oil and Natural Gas Wells by Production Rate*. www.eia.gov

Erik B, N. (2012). *Well cementing fundamentals*.

Humairah, S., Rahman, A., Medvedev, A., Yakovlev, A., Yon, S. ;, Sazali, A., Research, P., Bhd, S., Jain, B., Hassan, N., & Thompson, C. (2021). *IPTC-21371-MS Development of New Geopolymer-Based System for Challenging Well Conditions*. http://onepetro.org/IPTCONF/proceedings-pdf/21IPTC/4-21IPTC/D041S016R002/2424510/iptc-21371-ms.pdf

Kabir, I. I., Sorrell, C. C., Mada, M. R., Cholake, S. T., & Bandyopadhyay, S. (2016). General model for comparative tensile mechanical properties of composites fabricated from fly ash and virgin/recycled high-density polyethylene. *Polymer Engineering and Science*, *56*(10), 1096–1108. https://doi.org/10.1002/pen.24342

Kar, K. K. (2022). *Handbook of Fly Ash*.

Karim, M. R., Chowdhury, F. I., Zabed, H., & Saidur, M. R. (2018). Effect of elevated temperatures on compressive strength and microstructure of cement paste containing palm oil clinker powder. *Construction and Building Materials*, *183*, 376–383. https://doi.org/10.1016/j.conbuildmat.2018.06.147

Kurdowski, W. (2014). Cement and concrete chemistry. In *Cement and Concrete Chemistry* (Vol. 9789400779457). Springer Netherlands. https://doi.org/10.1007/978-94-007-7945-7

Lee, C. Y., Lee, H. K., & Lee, K. M. (2003). Strength and microstructural characteristics of chemically activated fly ash-cement systems. *Cement and Concrete Research*, *33*(3), 425–431. https://doi.org/10.1016/S0008-8846(02)00973-0

Luke, K. (2004). Phase studies of pozzolanic stabilized calcium silicate hydrates at 180 °C. *Cement and Concrete Research*, *34*(9), 1725–1732. https://doi.org/10.1016/j.cemconres.2004.05.021

Mahmoud, A. A., & Elkatatny, S. (2019). *temperature*.

Matsunaga, T., Kim, J. K., Hardcastle, S., & Rohatgi, P. K. (2002). Crystallinity and selected properties of fly ash particles. In *Materials Science and Engineering* (Vol. 325). www.elsevier.com/locate/msea

Misri, Z., Ibrahim, M. H. W., Awal, A. S. M. A., Desa, M. S. M., & Ghadzali, N. S. (2018). Review on factors influencing thermal conductivity of concrete incorporating various type of waste materials. *IOP Conference Series: Earth and Environmental Science*, *140*(1). https://doi.org/10.1088/1755-1315/140/1/012141

Norsok. (2013). *Well integrity in drilling and well operations, NORSOK Standard D-010*. www.standard.no/petroleum

Okoye, F. N., Durgaprasad, J., & Singh, N. B. (2015). Mechanical properties of alkali activated flyash/Kaolin based geopolymer concrete. *Construction and Building Materials*, *98*, 685–691. https://doi.org/10.1016/j.conbuildmat.2015.08.009

Poon, C. S., Kou, S. C., Lam, L., & Lin, Z. S. (2001). *Activation of fly ash/cement systems using calcium sulfate anhydrite (CaSO 4)*.

Rashad, A. M. (2015). An exploratory study on high-volume fly ash concrete incorporating silica fume subjected to thermal loads. *Journal of Cleaner Production*, *87*(1), 735–744. https://doi.org/10.1016/j.jclepro.2014.09.018

Renpu, W. (2011). *Advanced Well Completion Engineering*.

Rincon, F., Abid, K., Arbad, N., & Teodoriu, C. (2022). A comprehensive analysis of class H cement Unconfined Compressive Strength using cubical and cylindrical samples. *Journal of Petroleum Science and Engineering*, *215*. https://doi.org/10.1016/j.petrol.2022.110692

Rincon, F., Teodoriu, C., Tuttle, J., & Rickard, B. (2022). *Effect of Micro-Cellulose on Mechanical Properties of Class C and H Cement at Room and Elevated Temperature*.

Romero, M. (2020). *EVALUACIÓN A ESCALA DE LABORATORIO DEL DESEMPEÑO DE UNA LECHADA DE CEMENTACIÓN UTILIZANDO NANO-ZEOLITA*. https://repository.uamerica.edu.co/handle/20.500.11839/7829

Romero, M., Devers, C., & Teodoriu, C. (2022). *Observations of Thermal Cracking Propagation in Geopolymer Curing*. https://pangea.stanford.edu/ERE/db/GeoConf/papers/SGW/2023/Romero.pdf

Roshan, H. (2010). *Characteristics of Oilwell Cement Slurry Using CMC*. http://onepetro.org/DC/article-pdf/25/03/328/2090999/spe-114246-pa.pdf

Salazar, A. (2003). On thermal diffusivity. In *JOURNAL OF PHYSICS Eur. J. Phys* (Vol. 24). http://iopscience.iop.org/0143-0807/24/4/353

Salehi, S., Khattak, M. J., Ali, N., & Rizvi, H. R. (2016). *IADC/SPE-178793-MS Development of Geopolymer-based Cement Slurries with Enhanced Thickening Time, Compressive and Shear Bond Strength and Durability*. http://onepetro.org/SPEDC/proceedings-pdf/16DC/3-16DC/D031S025R007/1390118/spe-178793-ms.pdf/1

Sandl, E., Cahill, A. G., Welch, L., & Beckie, R. (2021). Characterizing oil and gas wells with fugitive gas migration through Bayesian multilevel logistic regression. *Science of the Total Environment*, *769*. https://doi.org/10.1016/j.scitotenv.2020.144678

Shafigh, P., Asadi, I., Akhiani, A. R., Mahyuddin, N. B., & Hashemi, M. (2020). Thermal properties of cement mortar with different mix proportions. *Materiales de Construccion*, *70*(339). https://doi.org/10.3989/mc.2020.09219

SLB. (2023). *Casing Energy Glossary*. https://glossary.slb.com/en/terms/c/casing

Teodoriu, C., Clausthal, T. U., Ugwu, I., Schubert, J., & A&m, T. (2010). *SPE 131335 Estimation of Casing-Cement-Formation Interaction using a new Analytical Model*. http://onepetro.org/SPEEURO/proceedings-pdf/10EURO/All-10EURO/SPE-131335-MS/1741736/spe-131335-ms.pdf

Thermtest Instrument. (2019). *What is Thermal Conductivity?* https://thermtest.com/what-is-thermal-conductivity

Trudel, E., Bizhani, M., Zare, M., & Frigaard, I. A. (2019). Plug and abandonment practices and trends: A British Columbia perspective. In *Journal of Petroleum Science and Engineering* (Vol. 183). Elsevier B.V. https://doi.org/10.1016/j.petrol.2019.106417

UK oil and Gas Industry Association. (2019). *Well Life Cycle Integrity Guidelines – Issue 4*.

Vu, M. H., Sulem, J., & Laudet, J. B. (2012). Effect of the curing temperature on the creep of a hardened cement paste. *Cement and Concrete Research*, *42*(9), 1233–1241. https://doi.org/10.1016/j.cemconres.2012.05.015

Wang, B. X., Zhou, L. P., Peng, X. F., Du, X. Z., & Yang, Y. P. (2010). On the specific heat capacity of CuO nanofluid. *Advances in Mechanical Engineering*, *2010*. https://doi.org/10.1155/2010/172085

Wang, W. C. (2017). Compressive strength and thermal conductivity of concrete with nanoclay under Various High-Temperatures. *Construction and Building Materials*, *147*, 305–311. https://doi.org/10.1016/j.conbuildmat.2017.04.141